NASA CR-72465

AN INVESTIGATION OF THE NICKEL OXIDE ELECTRODE

by

S. Lerner and H. N. Seiger

Prepared For

NATIONAL AERONAUTICS AND SPACE ADMINISTRATION

CONTRACT NAS 3-10608

GULTON INDUSTRIES, INC.
Research & Development Division
Metuchen, New Jersey

NASA CR-72465

FINAL REPORT

AN INVESTIGATION OF THE NICKEL OXIDE ELECTRODE

by

S. Lerner and H. N. Seiger

Prepared For

NATIONAL AERONAUTICS AND SPACE ADMINISTRATION

September 2, 1968

CONTRACT NAS 3-10608

LEWIS RESEARCH CENTER
Cleveland, Ohio

GULTON INDUSTRIES, INC.
Research & Development Division
Metuchen, N. J.

TABLE OF CONTENTS

TABLE OF CONTENTS (Continued)

LIST OF TABLES

LIST OF TABLES (Continued)

LIST OF FIGURES

LIST OF FIGURES (Continued)

ACKNOWLEDGEMENTS

The authors would like to acknowledge the help of Mr. Robert Van Wyck and his staff at Industrial Reactor Laboratories for their help in obtaining the neutron diffraction patterns, and to Drs. Philip Vaughan and Joseph Potenza of Rutgers University for their help in evaluating the neutron diffraction patterns and performing the pertinent calculations.

INTRODUCTION

The investigations performed under this contract included the following: (1) an intensive study of stabilization of positive electrode materials at elevated temperatures which included various formation procedures and the optimization of the additives found beneficial in previous work; (2) studies of utilization charge acceptance, oxygen evolution and cycling losses of sealed cells; and (3) the identification and characterization of the improved doped nickel oxide electrodes by X-ray diffraction and differential thermal analysis.

AN INVESTIGATION OF THE NICKEL OXIDE ELECTRODE

by

S. Lerner and H. N. Seiger

ABSTRACT

A two phase program was carried out. The first phase indicated that additions of 20 mole percent cobalt to the positive electrode significantly increased both its capacity and high temperature charge retention characteristics.

The second phase concerned itself with the structural differences between ordinary nickel oxide positives and those with the 20% cobalt additions. These characteristics were studied by use of DTA and X-ray diffraction techniques and indicated that there is a different mechanism for the conversion of β-NiOOH·20% Co to γ-NiOOH·20% Co then for β-NiOOH to γ-NiOOH.

I. OUTLINE OF PROGRAM

The program was divided into two parts. The first, involved the determination of the best metal additive in the optimum concentration to provide high temperature charge retention. This was a continuation of the work begun under Contracts NAS 3-4178 and NAS 3-7620.

The electrodes containing the optimum additive have been evaluated with respect to charge retention at elevated stand, charge acceptance, utilization, oxygen evolution, and cycling losses in sealed cells.

The second part of the program concerned itself with an effort to determine the method by which the additive improves the electrode properties. These studies were carried out by X-ray diffraction and differential thermal analysis. In addition, preliminary neutron diffraction data have been obtained.

A. DETERMINATION OF THE OPTIMUM ADDITIVE (Preliminary Evaluation)

1. Construction of Test Cells

a. Plates

Impregnating solutions consisting of $Ni(NO_3)_2 \cdot 6H_2O$ and 15, 17-1/2, 20, 22-1/2, 25, and 40 mole percent $Co(NO_3)_2 \cdot 6H_2O$ and 20 and 40 mole percent manganese nitrate (obtained as a 50% solution).

For each quantity and additive type, 45 positive electrodes were impregnated.

b. Stacks

Single positive electrodes were surrounded by two sintered cadmium negative electrodes with two layers of non-woven nylon serving as a separator and 34% KOH as the electrolyte.

2. Formation Procedure

The cells were formed in three cycles; each cycle consisted of:

a. Charge at C/10 for 16 hours.

b. Discharge at C/5 to 0.9 V.

3. Cycling to Maximum Capacity

After formation, the maximum capacity was determined. This was carried out by a 2 hour constant voltage charge with a 4C current limit and a C rate discharge to 0.9 V. The maximum capacity was considered to have been attained when two consecutive cycles indicated no increase in capacity by being within 5% of each other.

4. Temperature Stand

Forty-five cells from each additive type and level were cycled to maximum capacity, disassembled, and the positive placed in beakers of electrolyte. Nine positives were stored at each of the following temperatures: 0°, 25°, 40°, 60°, 80°, and 95°C. Three electrodes from each temperature stand were rebuilt and discharged at the C/2 rate to 0.9 V at intervals of 1, 3, and 7 days.

B. EVALUATION OF POSITIVE ELECTRODES WITH OPTIMUM ADDITIVE (Final Evaluation)

After establishing the optimum electrode with respect to stabilization, the following tests were performed:

1. Charge Acceptance

The three-plate cells were charged to 140% of positive capacity at the 1, 2, 4, 10, and 20 hour rates. The cells were then discharged at the C rate to 0.9 Volts. This test was performed three times on each of three cells at each charge rate. This test was performed on electrodes containing the optimum additive concentration and on control electrodes.

2. Determination of Utilization Factors at Various Rates of Discharge

All charges were done at the one (1) hour rate. Discharges were performed at the 10 minute, 1, 2, 5, and 10 hour rates. Capacities were determined to 0.6 V. Three samples of the improved electrodes and three samples of control electrodes were tested at each rate.

3. Determination of Utilization Factors for Depth of Discharge at 25, 40, 50, 75 and 100%

The three plate cell was charged and discharged at the C rate. After the initial charge, the cell was discharged for 15 minutes at the C rate. It was then charged for 15 minutes at the C rate, and finally discharged to 1.0 V at the C rate. This was repeated for a 24 minute discharge, a 30 minute discharge, etc. A comparison was made of the capacities obtained when discharging to 1.0 V versus the various depths of discharge. Again, three samples of the improved and control electrodes were tested at each rate.

4. Oxygen Evolution

The oxygen evolution tests were performed in a specially designed laboratory test cell. The cell consisted of a metal can fitted with a lucite cover. A pressure transducer was used to measure the pressure. The oxygen evolution point at the 1, 2, 5, and 10 hour rates were determined.

5. Establishment of Optimum Formation Technique

Formation studies have been carried out as a function of rate and temperature in addition to cycle and reverse formation procedures.

6. Cycling Losses

Five sealed cells containing the improved electrodes, and five control cells were constructed. The cells were cycled to a 50% depth of discharge at the C rate for 200 cycles. On the 201st cycle, the cells were discharged for capacity.

C. STRUCTURAL STUDIES

1. X-ray Diffraction

Upon determining the optimum additive concentration level, electrodes both with and without additive were fabricated. The electrodes were charged to between 0 and 550% (0, 80, 100, 200, 550%) of capacity, X-rayed at each state of charge, and the structure of the electrodes containing the additive compared to that of the electrodes without the additive.

2. Differential Thermal Analysis (DTA)

In order to determine the chemical effect of additives on the nickel oxide electrodes, DTA measurements were performed on electrodes, both with and without additives, at various states of charge and overcharge (unformed to 550%).

3. Neutron Diffraction

Preliminary neutron diffraction patterns were obtained at Industrial Reactor Laboratories, Plainsboro, N. J.

II. EXPERIMENTAL PROCEDURES, RESULTS, & DISCUSSION

A. DETERMINATION OF OPTIMUM ADDITIVE (Preliminary Evaluation)

1. Impregnation

Solutions of $Ni(NO_3)_2 \cdot 6H_2O$ containing 0, 15, 17-1/2, 20, 22-1/2, 25, and 40 mole percent $Co(NO_3)_2 \cdot 6H_2O$ and 0, 20, and 40 mole percent $Mn(NO_3)_2$ were prepared. Forty-five plates were vacuum impregnated with each additive. The nitrate was then converted to the active hydroxide with potassium hydroxide.

2. Formation

The formation procedure for all cells consisted of 3 cycles. Each cycle consisted of a C/10 charge for 16 hours and a C/5 discharge to 0.9 V. A complete discharge curve was obtained on the last cycle. The formation procedure was identical for all test cells in the program.

Figures 1-4 are typical discharge curves for 0, 20, and 40 mole percent cobalt and 20% manganese. Tables I-IX are the formation capacities of all the cells investigated under this phase of the program.

3. Cycling to Maximum Capacity

All cells were cycled in the following manner: two hour constant potential charge at 1.6 V/cell with a maximum current of 3.2C, followed by a C rate discharge to 0.9 V. The cells were cycled until the average capacities on two successive cycles were within 5 to 6% of each other. A minimum of 3 cycles was used.

Tables X-XVI are the average capacities after constant voltage cycling of all the cells tested in this investigation with the exception of 40 mole percent cobalt and manganese which had formation capacities so low as to eliminate them from consideration (Tables VII and IX). Table XVII is a summary of the theoretical and experimental data on formation and cycling.

To determine the ampere-hour input for a 1.6 V/cell charge for two hours, the following method was used. A curve of charge current versus time was plotted on the same graph as a curve representing 1 Ah. This curve is shown in Figure 5. The two curves were then cut out and weighed on an analytical balance. Two determinations yielded an input of 1.75 Ah.

4. Temperature Scand

After completion of the cycling, each group of 45 cells was divided into three groups of 15, which were charged at 1.6 V/cell for two hours. Each group of 15 cells was designated for a 1, 3, or 7 day stand. Further, each group of 15 cells was subdivided into groups of three cells which were to stand at five different temperatures. After charging, the cells were disassembled and the positives stored in battery electrolyte. Nine positives of each additive type were stored at the following temperatures: 20°, 40°, 60°, 80° and 95°C. Three cells of each additive group were removed at 1, 3, or 7 day intervals, reassembled, and discharged to 0.9 V. These data are shown in Tables XVIII to XX for all cells except the 40% cobalt and manganese, which were not tested due to their low capacity.

As is readily discernable from these tables, the percentage loss of capacity on stand for the cobalt plates is about half that of the manganese and control plates. It was also found, upon disassembly of the cells, that in the case of the manganese additions, the separator had become impregnated with MnO_2 which was formed during the charging process and then leached out of the plates. The MnO_2 precipitated on the separator is, apparently, not reconverted to Mn^{+2} during discharge, and therefore, may contribute to a degradation of the separator material.

On the basis of the preliminary tests, positive electrodes containing 20 mole percent cobalt were chosen for final evaluation. The selection of 20% cobalt was made on the basis of the data correlation in Tables XVII to XX. The tables show that the 20% addition has, by far, the best capacity and has as good charge retention as any addition but the 22-1/2%. However, it was felt that the large gain in capacity of the 20% material outweighs the small difference in temperature stability.

B. EVALUATION OF POSITIVE ELECTRODES WITH OPTIMUM ADDITIVE (Final Evaluation)

1. Charge Acceptance

Six cells were constructed; three with control positives and three with 20% cobalt positives. The cells were charged to 140% of capacity at the 1, 2, 4, 10, and 20 hour rates and then discharged at the 1 hour rate to 0.9 V. The percent charge acceptance was based on the capacity obtained after the C rate charge, since high rate charges are most efficient. The results are summarized in Table XXI and Figure 6.

2. Utilization at Various Rates of Discharge

Six cells, three with control positives and three with 20% cobalt positives, were tested in the following manner. The cells were charged to 150% capacity at the C rate and then discharged to 0.9 V at the C/10, C/4, C/2, C/1, and 6C/1 rates. The results are shown in Figure 7. Since the utilization of the 20% cobalt positives appeared to be low at high rates, an additional test was performed where the cells were discharged to 0.6 V at the higher rates. These results are shown in Figure 8.

It can be seen in Figure 8 that at rates between 4000 mA (4C) and 1000 mA (C), the cobalt positives show a significantly better utilization than the control positives when discharged to 0.6 V. At rates higher than 4C and lower than C, however, the two groups have similar utilizations of capacity. Obviously there is a good deal of capacity available in the 20% cobalt positives between 0.9 and 0.6 volt at these higher rates.

3. Utilization at Various Depths of Discharge

Three control and three 20% cobalt cells were fabricated and tested in the following manner: (All charges and discharges were performed at the C rate.)

The cells were charged to 150% of capacity, discharged for 15 minutes (25% DOD), charged for 15 minutes, and then discharged to 1.0 V. This was repeated for 24 minutes (40% DOD), 30 minutes (50% DOD), 45 minutes (75% DOD), and 60 minutes (100% DOD). The results are shown in Table XXII.

These results indicate that the differences between the control and 20% cobalt positives are of no practical significance.

4. Oxygen Evolution

The rate, and point in the charge curve at which the positive electrode in a nickel-cadmium cell begins to generate oxygen, is a measure of the efficiency of the electrode. In order to determine this efficiency, the following experiment was performed. A laboratory cell with a removable top was fabricated. The top was fitted with three terminals and a pressure transducer. Two positive counter electrodes were connected to the negative terminal, the single test electrode of known capacity was connected to the positive terminal, and a blank screen to the third terminal. The cell was flooded with electrolyte--the amount adjusted so the free volume of the cell was 30 cc. With the cell in a vented condition, the electrodes at the negative terminal were charged versus the blank electrode. At the end of charge, the cell was sealed and evacuated, and the test electrode was charged versus the two counter electrodes, and the pressure rise monitored by the pressure transducer. From the plot of pressure versus time, the point of vigorous gassing and the fraction of the charge current producing the gassing, may be determined. The fraction of the total current producing the parasitic (gassing) reaction may be calculated from the following equation:

$$I_{O_2} = \frac{4FV}{RT} \frac{dP}{dt}$$

Figures 9-13 are the oxygen evolution curves expressed as percent of charging current producing oxygen versus state of charge for charge currents of 1/10, 1/2, 1, 2 and 6 amperes respectively. Except at 100 mA (C/10), the positives with 20% cobalt reached a 10-20% higher state of charge than the control cells before the onset of vigorous gassing, thus indicating a more efficient electrode.

The greater efficiency of the 20% cobalt positive is dramatically demonstrated at the 10 hour rate where charging is known to be rather inefficient. At that rate, the control electrode gasses rapidly almost immediately while the 20% cobalt electrode does not begin to gas vigorously until it is 60% charged.

5. Establishment of Optimum Formation Technique

Thirty cells with 20% cobalt positives were constructed for use in evaluating various formation techniques. Twenty cells were used to evaluate the effect of rate and temperature, five cells were used to evaluate a cycle type formation, and five to evaluate a reverse type formation.

a. Effect of Rate and Temperature

Twenty cells with cobalt positives were constructed. Five cells were formed at C/10-25°C, five at C/30-25°C, five at C/10-10°C, and five at C/30-10°C. Each cell was given three cycles and the average capacity on the last cycle is shown in Table XXIII. It is apparent that those cells formed at low rates and temperatures exhibit a slightly greater capacity than those formed at C/10 and room temperature. However, it has been shown that this formation procedure causes no significant differences with respect to stability at room or elevated temperatures.(1)

b. Cycle Formation

The cycle formation consisted of a C/10 charge for 50 minutes of each hour and a C/5 discharge for 10 minutes of each hour. The total time on cycle was 32 hours which is equivalent to 160% charge. The cells were discharged at the C/10 rate to 0.0 V. The results, for the 3rd cycle shown in Table XXIV, indicate that this type of formation results in lowered capacity.

c. Reverse Formation

The reverse formation consisted of a C/10 charge to 160% of capacity and a C/10 discharge to -1.5 V. On the final cycle (3rd), the cells were discharged to 0.0 V. The results, shown in Table XXV, indicate that this method of formation leads to rather high capacities being only slightly lower than those obtained when the formation is carried out at C/30-10°C.

6. Sealed Cell Cycling

a. Group I

Ten, six ampere-hour laboratory cells were fabricated. Five cells (nos. 336-340) contained control positive electrodes, and five cells (nos. 341-345) contained positive electrodes with 20% cobalt. The cells were placed on automatic cycle at 50% depth of discharge, using a 90 minute (60 minute charge; 30 minute discharge) orbit with a 10% overcharge. The cells were cycled for a total of 200 cycles.

From the start of cycling, the pressures in the cobalt cells were significantly higher than those in the control cells, and there was almost no recombination on the discharge portion of the cycle. At the end of the 36th cycle, it became apparent that the pressure was increasing (averaging 75 psia/cell as compared to 25 psia/cell for the controls) with each cycle, rather than reaching a stable value.

The cells were removed from charge and the gas analyzed. The analysis indicated large amounts of hydrogen. To overcome this problem, the negative electrodes were predischarged 0.2 Ah by the addition of 65 psia of oxygen, placed back on cycle, and allowed to complete the required 200 cycles. During the remaining cycles, the cells operated at moderately high pressures ($\sim$ 65 psia) but became stabilized after a few cycles.

When cycling was terminated, the control cells had completed 202 cycles with all cell voltages below 1.0 volt, and the 20% cobalt cells had completed 211 cycles with all cell voltages above 1.0 V. The final cycles for each set of cells is summarized in Table XXVI along with the total useful capacity of the cobalt cells.

It is speculated that the extra capacity in the cobalt containing positives allowed the cells to become negative limiting, thereby resulting in high hydrogen pressures.

One cell with cobalt positives was placed on continuous 50% depth of discharge cycle after the negative electrodes had been further predischarged with oxygen. This cell had been on continuous cycle and had completed more than 1800 cycles when the pressure began to become excessive ($>$ 50 psig). The cell was removed from cycle, reconditioned, and replaced on cycle. To date, the cell has completed 1168 cycles after reconditioning, and a total of 4200 cycles. It is presently operating in the pressure range of 8-12 psia, with an end of discharge voltage of 1.10 V.

The cell reconditioning procedure consisted of the following: At the conclusion of the 1834th cycle, the cell was discharged to 0.0 V at the C rate. The cell was shorted for 6 hours, charged at the C/10 rate (sealed) for 16 hours, discharged at the C/2 rate to 1.0 V, charged at the C/2 rate for 3 hours, discharged at the C rate to 1.0 V, charged at C/2 for 3 hours, and then replaced on cycle.

b. Group II

Due to the high pressures exhibited in the cells with 20% cobalt positives, a second group of cells was prepared as follows:

(1) Impregnation

Eighty electrodes were impregnated with $Ni(NO_3)\cdot 6H_2O$ containing 20 mole percent cobalt. After conversion to the hydroxide, the plates contained an average of approximately 3 grams each of $Ni(OH)_2\cdot$20% Co. For use in control cells, 80 positive electrodes from the Gulton Plate Facility were obtained. These electrodes averaged 3.4 grams of active material. All negative electrodes were obtained from the Gulton Plate Facility.

(2) Physical Properties

The porosity of 10 electrodes of both types were determined by alcohol absorption. In addition to the porosity, both the weight and thickness of the plates were determined. The test data are shown in Table XXVII. It is obvious that the porosity of the cobalt positives is somewhat lower than that of the control positives. This fact may be related to the high pressure in the cobalt cells which were previously cycled. This comes about since the same amount of electrolyte was used for both types of cells, and since the porosity of the cobalt positives is lower, this may have led to a less dry cell condition.

(3) Formation

The electrodes were constructed into cell packs and formed at the C/10 rate, i.e., a C/10 charge for 16 hours followed by a C/10 discharge to 1.0 V. Three such cycles were performed. Table XXVIII lists the formation capacity of the cell packs on the final formation cycle. On the basis of the formation, it was decided to consider the cobalt cells as 5 Ah cells and the controls as 6 Ah cells for future test purposes. This difference in capacity is to be expected as capacity is proportional to loading.

(4) Sealed Cell Cycling

Five cells of each type were constructed. Two cells of each type had reference electrodes for monitoring the positive and negative electrode behavior during cycling. The cells were placed on an automatic cycling regime to 50% depth of discharge with a 110% reinsertion. To date, the cells have completed over 2000 cycles. Table XXIX illustrates the end of charge and end of discharge characteristics for all cells at the 800th cycle.

The most significant fact is that the control cells are beginning to have end of charge voltages below 1.00 V, which indicates the onset of the memory effect. In addition, while the pressures at the 800th cycle are about the same for both sets of cells, the control cells have had excursions into severely elevated pressures ($>$90 psia) and had to be vented early in the cycling (cycle 220).

C. STRUCTURAL STUDIES

Structural studies have been carried out by the techniques of X-Ray Diffraction, Differential Thermal Analysis (DTA), and some preliminary neutron diffraction studies.

1. X-Ray Diffraction and Differential Thermal Analysis

X-ray diffraction patterns and DTA thermograms were run on both control positives and positives with 20% cobalt at the following states of charge: 0, 90, 100, 150, 200, and 600%.

a. $Ni(OH)_2$ (Control) Positives

Figures 14 through 19 are the X-ray diagrams for the control positives. These electrodes show the same X-ray structures as previously described[2], going from crystalline $Ni(OH)_2$ structure to the amorphous β-NiOOH structure to the recrystallized γ-NiOOH structure. The thermograms are shown in Figures 20 through 25. As the charged state evolves, the endotherm above 200°C, which corresponds to the dehydroxylation of $Ni(OH)_2$, is seen to decrease as the material is converted to β-NiOOH. However, even in the highly overcharged material, this feature is still present to some degree, indicating some features of the basic $Ni(OH)_2$ structure are retained. As overcharge continues, two additional endotherms at 140° and 190°C become sharply defined. This has been shown to indicate the presence of discretely bound species.[3]

A third feature, evident in the thermograms of the 150% and 200% charged materials, is the large exotherm at 320° to 330°C. This is associated with the recrystallization of the amorphous β-NiOOH as it is converted to NiO. This feature is absent from the 600% charged material since the active material is again crystalline and the dehydroxylation endotherm is again evident.

b. $Ni(OH)_2$ 20% Cobalt (Experimental) Positives

The X-ray patterns of positives containing 20% cobalt (Figures 26 through 31) show, generally, a more amorphous structure in the lower states of charge (0-150%). This amorphousness indicates decreased crystallite size, thereby yielding an increase in surface area, and thus, an increase in reactivity which may account for the greater capacity of the cobalt containing positives. At the 200% charged state, the electrode has the highly crystalline $Ni(OH)_2$ structure, and at 600% charged, both the $Ni(OH)_2$ and the γ-NiOOH structures are present.

The DTA thermograms shown in Figures 31 through 37 show some differences from the corresponding thermograms of the undoped positives.

At 0% charged, the thermogram is very similar to that of $Ni(OH)_2$, i.e., endotherms at 150 and 300°C. As the charged state develops, the endotherms at 150°C (the loss of loosely bound water) and 300°C (dehydroxylation) decrease rapidly while a third endotherm at about 200° rapidly increases. This endotherm is associated with the charged state and has been associated with discretely bound species.[2] It is of interest that the endotherm at 200°C develops at a lower state of charge when cobalt is present. This would agree with other data that, for a given coulombic input, the doped positives are at a greater state of charge than the undoped positives, due to their more efficient charge acceptance. At 200% charged, the X-ray pattern indicated a crystalline $Ni(OH)_2$ type structure. This is confirmed by the thermogram which is very similar to that of a discharged electrode. At 600% charged, the thermogram shows evidence of both the charged state (endotherm at 195°C) and the discharged $[Ni(OH)_2]$ state (endotherm at 146° and 310°C).

However, the main difference between the thermograms of the doped and undoped electrodes is the absence of the intense exotherm which appears at 320° in the undoped electrodes at the 150 and 200% charged states. Since the 200% charged state of the cobalt containing positive is crystalline, it is obvious why the exotherm is not present. However, its absence in the amorphous 150% charged electrode indicates a mechanism for the conversion of β-NiOOH · 20% Co to γ-NiOOH · 20% Co different from that for the conversion β-NiOOH to γ-NiOOH.

2. Neutron Diffraction

It has been previously postulated[4] that there is little structural change in the positive electrode with state of charge until almost full charge has been reached, since the chemical change is small, involving only the loss of a proton in going from $Ni(OH)_2$ to β-NiOOH. The use of X-ray techniques cannot resolve this hypothesis since protons are invisible to X-rays. However, the use of neutron diffraction techniques should resolve this problem, since the effect of protons on the intensity of various reflections is large. Table XXX shows the effect of the loss of one-half of the protons $[Ni(OH)_2 \xrightarrow{\bullet} \beta\text{-NiOOH} + H^+]$ on the intensity at selected reflections. Figure 38 is a typical neutron diffraction pattern for a positive electrode which has never seen current or electrolyte.

D. CONCLUSIONS

From the preliminary evaluation, it was apparent that the best positives are those with additions of 20% cobalt. It was also apparent that the addition of manganese at the 20% level did not lead to significant improvement.

Utilization studies indicate that there is little difference between 20% cobalt positives and control positives as a function of depth of discharge. However, as a function of rate, at high rates (>3C), the cobalt containing positives have to be discharged to 0.6 V to perform as well as control positives discharged to 0.9 V. At rates lower than 3C, both types of positives perform equally as well to 0.9 V.

Charge acceptance and oxygen evolution studies (both of which are a measure of positive electrode efficiency) indicate that at all charge rates, the 20% cobalt containing positives are more efficient electrodes than the control positives.

The X-ray and DTA studies, along with charge acceptance and oxygen evolution, have indicated several reasons for the greater capacity of positive electrodes with cobalt additives. These are: (1) greater reactivity due to small particle size and the concurrent increase in surface area, and (2) the more efficient charge acceptance of the cobalt doped plates, i.e., for the same coulombic input, the doped plates are at a higher state of charge than the undoped control electrodes.

The results of the sealed cell testing indicate that cells using cobalt positives are better able to withstand the rigors of deep depth of discharge (50%) cycling, under short orbit conditions, than cells with control electrodes.

In addition, the cells with cobalt containing positives do not appear as susceptible to the memory effect as cells with undoped positive electrodes.

E. SUGGESTIONS FOR FUTURE INVESTIGATIONS

The most logical line of future work would seem to be a continuation of the investigation of the structure of the positive electrode by neutron diffraction techniques.

III. REFERENCES

(1) Ritterman, P., Lerner S, and Seiger, H. - "Investigation of Battery Active Nickel Oxides", Third Quarterly Report, NASA CR-54957, Contract NAS 3-7620, March 12, 1966.

(2) Ritterman, P., Lerner, S. and Seiger, H.N. - "Investigation of Battery Active Nickel Oxides", Final Report, Contract NAS 3-7620, September 12, 1966.

(3) Aia, M. A. - "Structure and Stoichiometry of Nickel Hydroxides in Sintered Nickel Positive Electrodes", ECS Meeting, Fall 1966.

(4) Ritterman, P., Lerner, S., Seiger, H. N. and Vaughan, P. A. "The Structure of Battery Active Nickel Oxides Existing on the Sintered Plate Nickel Oxide Electrode at Various States of Charge", ECS Meeting, Fall 1966.

T A B L E S

TABLE I

FORMATION CAPACITIES - CONTROL CELLS

DISCHARGED C/5

CELL NO.	CAPACITY mAh	CELL NO.	CAPACITY mAh	CELL NO.	CAPACITY mAh
1	740	16	716	31	720
2	743	17	737	32	725
3	750	18	674	33	833
4	727	19	720	34	756
5	705	20	745	35	705
6	711	21	759	36	795
7	725	22	732	37	792
8	705	23	735	38	762
9	705	24	748	39	780
10	713	25	725	40	783
11	748	26	759	41	773
12	740	27	727	42	789
13	745	28	708	43	786
14	737	29	730	44	780
15	750	30	693	45	776

TABLE II

FORMATION CAPACITIES 15% COBALT

DISCHARGED C/5

CELL NO.	CAPACITY mAh	CELL NO.	CAPACITY mAh	CELL NO.	CAPACITY mAh
136	950	151	942	166	866
137	916	152	896	167	882
138	930	153	882	168	836
139	966	154	882	169	852
140	946	155	892	170	896
141	850	156	832	171	892
142	890	157	890	172	872
143	942	158	850	173	862
144	922	159	840	174	880
145	900	160	860	175	860
146	872	161	882	176	916
147	900	162	880	177	892
148	926	163	836	178	896
149	900	164	882	179	910
150	882	165	882	180	846

TABLE III

FORMATION CAPACITIES - 20% COBALT

DISCHARGED C/5

CELL NO.	CAPACITY mAh	CELL NO.	CAPACITY mAh	CELL NO.	CAPACITY mAh
1	882	16	822	31	906
2	960	17	860	32	896
3	916	18	876	33	930
4	922	19	916	34	922
5	940	20	906	35	900
6	922	21	920	36	910
7	896	22	922	37	900
8	900	23	926	38	912
9	896	24	926	39	926
10	890	25	876	40	912
11	896	26	902	41	922
12	850	27	950	42	932
13	890	28	920	43	872
14	900	29	906	44	872
15	846	30	896	45	922

TABLE IV

FORMATION CAPACITIES - 17½% COBALT

DISCHARGED C/5

CELL NO.	CAPACITY mAh	CELL NO.	CAPACITY mAh	CELL NO.	CAPACITY mAh
181	936	196	936	211	830
182	952	197	982	212	850
183	976	198	962	213	830
184	946	199	932	214	866
185	970	200	970	215	892
186	970	201	960	216	832
187	956	202	946	217	882
188	922	203	1020	218	900
189	922	204	916	219	900
190	950	205	916	220	866
191	990	206	860	221	860
192	862	207	910	222	852
193	910	208	892	223	860
194	942	209	850	224	866
195	930	210	886	225	860

TABLE V

FORMATION CAPACITIES - 22½% COBALT

DISCHARGED C/5

CELL NO.	CAPACITY mAh	CELL NO.	CAPACITY mAh	CELL NO.	CAPACITY mAh
226	Short	241	882	256	962
227	910	242	832	257	886
228	860	243	890	258	960
229	814	244	910	259	966
230	850	245	942	260	982
231	882	246	832	261	880
232	850	247	906	262	866
233	862	248	900	263	842
234	890	249	990	264	842
235	892	250	962	265	916
236	886	251	962	266	862
237	932	252	922	267	860
238	920	253	952	268	866
239	860	254	952	269	896
240	886	255	966	270	850

TABLE VI

FORMATION CAPACITIES - 25% COBALT

DISCHARGED C/5

CELL NO.	CAPACITY mAh	CELL NO.	CAPACITY mAh	CELL NO.	CAPACITY mAh
91	850	106	808	121	876
92	840	107	816	122	852
93	796	108	840	123	876
94	850	109	850	124	880
95	794	110	814	125	830
96	866	111	784	126	866
97	846	112	808	127	872
98	836	113	856	128	866
99	820	114	796	129	866
100	832	115	860	130	856
101	840	116	846	131	866
102	800	117	866	132	882
103	770	118	832	134	902
104	788	119	846	135	846
105	816	120	890		

TABLE VII

FORMATION CAPACITIES - 40% COBALT

DISCHARGED C/5

CELL NO.	CAPACITY mAh	CELL NO.	CAPACITY mAh	CELL NO.	CAPACITY mAh
46	520	61	500	76	*
47	536	62	500	77	*
48	522	63	506	78	*
49	532	64	506	79	*
50	532	65	*	80	*
51	506	66	*	81	506
52	520	67	526	82	506
53	532	68	526	83	506
54	532	69	520	84	506
55	496	70	506	85	520
56	520	71	506	86	*
57	520	72	506	87	520
58	520	73	*	88	506
59	520	74	*	89	506
60	492	75	*	90	520

* Plates Not Usable

TABLE VIII

FORMATION CAPACITIES - 20% MANGANESE

DISCHARGED C/5

CELL NO.	CAPACITY mAh	CELL NO.	CAPACITY mAh	CELL NO.	CAPACITY mAh
1	882	16	822	31	906
2	900	17	860	32	896
3	916	18	876	33	930
4	922	19	916	34	922
5	940	20	906	35	900
6	922	21	920	36	910
7	896	22	922	37	900
8	900	23	926	38	912
9	896	24	926	39	926
10	890	25	876	40	912
11	896	26	902	41	922
12	850	27	950	42	932
13	890	28	920	43	872
14	900	29	906	44	872
15	846	30	896	45	922

TABLE IX

FORMATION CAPACITIES - 40% MANGANESE

DISCHARGED C/5

CELL NO.	CAPACITY mAh	CELL NO.	CAPACITY mAh	CELL NO.	CAPACITY mAh
46	570	61	580	76	550
47	556	62	580	77	536
48	572	63	570	78	570
49	550	64	582	79	576
50	560	65	600	80	562
51	572	66	526	81	516
52	540	67	536	82	562
53	562	68	572	83	552
54	552	69	552	84	526
55	586	70	542	85	556
56	582	71	536	86	532
57	576	72	512	87	520
58	556	73	540	88	550
59	572	74	540	89	550
60	562	75	552	100	552

TABLE X

AVERAGE CAPACITIES AFTER CONSTANT VOLTAGE CYCLING

CONTROL CELLS

DISCHARGED AT C/1

GROUP	CYCLE I	CYCLE 2	CYCLE	CYCLE 4
1 - 15	747	779	822	819
16 - 30	780	813	82[illegible]	826
31 - 45	798	794	7[illegible]	797

TABLE XI

AVERAGE CAPACITIES AFTER CONSTANT VOLTAGE CYCLING
15% COBALT

DISCHARGED C/1

GROUP	CYCLE 1	CYCLE 2	CYCLE 3
136-150	853	844	866
151-165	867	855	891
166-180	943	915	938

TABLE XII

AVERAGE CAPACITIES AFTER CONSTANT VOLTAGE CYCLING
17-1/2% COBALT

DISCHARGED C/1

GROUP	CYCLE 1	CYCLE 2	CYCLE 3
181-195	837	845	864
196-210	862	865	872
211-225	831	845	863

TABLE XIII

AVERAGE CAPACITIES AFTER CONSTANT VOLTAGE CYCLING - 20% COBALT

DISCHARGED AT C/1

GROUP	CYCLE 1	CYCLE 2	CYCLE 3
1 - 15	877	955	933
16 - 30	892	936	961
31 - 45	952	962	957

TABLE XIV

AVERAGE CAPACITIES AFTER CONSTANT VOLTAGE CYCLING

22½% COBALT

DISCHARGED C/1

GROUP	CYCLE 1	CYCLE 2	CYCLE 3
226 - 240	836	840	872
241 - 225	803	818	836
256 - 270	846	852	855

TABLE XV

AVERAGE CAPACITIES AFTER CONSTANT VOLTAGE CYCLING - 25% COBALT

DISCHARGED C/1

GROUP	CYCLE 1	CYCLE 2	CYCLE 3
91 - 105	800	779	797
106 - 120	793	772	800
121 - 135	793	836	829

TABLE XVI

AVERAGE CAPACITIES AFTER CONSTANT VOLTAGE CYCLING - 20% MANGANESE

DISCHARGED C/1

GROUP	CYCLE 1	CYCLE 2	CYCLE 3
1 - 15	693	728	678
16 - 30	619	670	684
31 - 45	707	658	650

TABLE XVII

COMPARISON OF THEORETICAL AND ACTUAL CAPACITIES

	THEORETICAL CAPACITY TOTAL WEIGHT	THEORETICAL CAPACITY	MEASURED CAPACITY	MEASURED CAPACITY
	AS $Ni(OH)_2$	$Ni(OH)_2$ ONLY	FORMATION	C.P.C.
CONTROL	790	790	742	813
15% CO	948	858	889	898
17½% CO	892	737	910	866
20% CO	865	694	902	948
22½% CO	881	683	899	854
25% CO	881	662	840	809
40% CO	867	520	515	--
20% Mn.	861	691	722	671
40% Mn.	798	479	556	--

CPC = CONSTANT POTENTIAL CHARGE

TABLE XVIII

PERCENT LOSS IN CAPACITY - 1 DAY STAND

CELLS	TEMPERATURE				
	R.T.	40°C	60°C	80°C	95°C
CONTROL	4	5	18	38	28
15% Co	10	11	6	23	24
17-1/2% Co	3	3	5	3	12
20% Co	4	4	12	13	--
22-1/2% Co	1	1	7	9	12
25% Co	1	13	--	13	19
40% Co		CELLS NOT TESTED			
20% Mn	1	10	16	20	22
40% Mn		CELLS NOT TESTED			

TABLE XIX

PERCENT LOSS IN CAPACITY - 3 DAY STAND

CELLS	TEMPERATURE				
	R. T.	40°C	60°C	80°C	95°C
CONTROL	8	0	22	57	42
15% Co	10	13	14	28	28
17-1/2% Co	12	10	8	14	26
20% Co	4	7	14	16	20
22-1/2% Co	--	1	8	5	12
25% Co	0	6	7	18	15
40% Co	CELLS NOT TESTED				
20% Mn	10	15	20	17	37
40% Mn	CELLS NOT TESTED				

TABLE XX

PERCENT LOSS IN CAPACITY - 7 DAY STAND

CELLS	TEMPERATURE				
	R. T.	40°C	60°C	80°C	95°C
CONTROL	2	4	12	37	36
15% Co	8	10	17	8	25
17-1/2% Co	6	2	7	7	13
20% Co	4	12	10	17	14
22-1/2% Co	1	9	8	8	15
25% Co	3	7	1o	18	13
40% Co			CELLS NOT TESTED		
20% Mn	9	15	29	39	41
40% Mn			CELLS NOT TESTED		

TABLE XXI

CHARGE ACCEPTANCE

	CAPACITY (mAh)	CAPACITY (mAh)	% OF C RATE	% OF C RATE
CHARGE RATE	CONTROLS	20% Co	CONTROLS	20% Co
C	750	876	100	100
C/2	739	856	98	98
C/4	723	852	96	97
C/10	697	840	90	96
C/20	579	849	77	97

TABLE XXII

UTILIZATION AT VARIOUS DEPTHS OF DISCHARGE (DOD)

% CAPACITY AS A FUNCTION OF DOD

CELLS	DOD	0	25	40	50	75	100
CONTROLS		100	92	93	95	92	95
20% COBALT		100	94	91	96	88	92

TABLE XXIII

FORMATION CAPACITY AS A FUNCTION OF RATE AND TEMPERATURE

CAPACITY IN mAh

20% COBALT POSITIVES

C/10-25°C	C/10-10°C	C/30-25°C	C/30-10°C	% CHANGE
904	902			0
904		868		-4
904			966	+7

TABLE XXIV

CYCLE FORMATION

CELL	CAPACITY mAh TO 0.0V
71	783
72	783
73	771
74	750
75	745

TABLE XXV

REVERSE FORMATION

CELL	CAPACITY mAh TO 0.0V
80	915
81	858
82	965
83	918
84	921

TABLE XXVI

FINAL CYCLE, SEALED CELL CYCLING (1)

CELLS	END CHARGE VOLTAGE	END CHARGE PSIA	END DISCHARGE VOLTAGE	END DISCHARGE PSIA	CAPACITY TO 1.0V FOLLOWING LAST CYCLE
CONTROLS:					
336	1.48	21	0.99	15	---
337	1.51	37	0.80	31	---
338	1.50	30	0.68	24	---
339	1.48	25	0.66	21	---
340	1.48	21	0.72	15	---
COBALT:					
341	1.54	66	1.11	59	5.20
342	1.53	75	1.11	69	5.20
343	1.53	65	1.09	59	4.70
344	1.56	52	1.01	50	3.40
345	1.52	50	1.08	49	4.70

TABLE XXVII

PHYSICAL PROPERTIES OF ELECTRODES

CONTROL	WT. (Gms)	THICKNESS (in.)	POROSITY (%)	COBALT	WT. (Gms)	THICKNESS (in.)	POROSITY (%)
1	7.90	0.0310	14.8	1	7.55	0.0305	13.2
2	7.98	0.0325	14.8	2	7.54	0.0320	10.2
3	7.93	0.0320	15.1	3	7.56	0.0315	14.1
4	7.78	0.0310	17.1	4	7.53	0.0305	10.6
5	7.96	0.0325	14.9	5	7.58	0.0305	11.2
6	7.90	0.0315	14.9	6	7.61	0.0305	13.1
7	7.98	0.0320	14.8	7	7.60	0.0305	12.2
8	7.94	0.0325	15.0	8	7.56	0.0320	13.1
9	7.90	0.0310	14.8	9	7.60	0.0305	10.6
10	7.96	0.0320	15.0	10	7.59	0.0315	12.4
Avg	7.87	0.0318	15.1	Avg	7.57	0.0310	12.1

TABLE XXVIII

FORMATION CAPACITIES OF CELL PACKS TO 1.0 V

(THIRD CYCLE)

CELLS		AMPERE-HOURS
1	Cobalt	5.73
2	Cobalt	5.93
3	Cobalt	5.82
4	Cobalt	5.80
5	Cobalt	5.73
6	Cobalt	5.65
7	Cobalt	5.80
8	Control	6.20
9	Control	6.35
10	Control	6.63
11	Control	6.63
12	Control	6.63
13	Control	6.50
14	Control	6.45

TABLE XXIX

SEALED CELL CYCLING - CYCLE 800

CELLS	END CHARGE VOLTAGE	END CHARGE PSIA	END DISCHARGE VOLTAGE	END DISCHARGE PSIA
CONTROLS:				
356	1.48	40	0.98	35
357	1.48	31	0.98	27
358	1.48	23	1.00	19
359	1.49	17	0.96	11
360	1.49	21	1.02	18
COBALT:				
351	1.51	40	1.12	35
352	1.50	28	1.13	23
353	1.50	30	1.12	25
354	1.52	28	1.13	21
355	1.51	38	1.13	32

TABLE XXX

SOME CALCULATED NEUTRON DIFFRACTION INTENSITIES * FOR $Ni(OH)_2$

hkl	d_{calc}	I_H	$I_{1/2H}$	% CHANGE
001	4.62	6.2	3.9	37
100	2.70	4.1	2.5	41
101,002	2.31, 2.33	15.0	19.2	28
$102,10\bar{2}$ **	1.75	46.5	38.3	18
110,003,111	1.56,1.54,1.47	54.6	46.6	15

* All intensities are on the same scale. I_H was calculated from from the formula $I_H = \sum m_{hkl} F^2(hkl)$, where m is the multiplicity of the hkl plane and the sum is over the distinct planes indicated in the table. For neutron diffraction, $f_{Ni} = 1.03$, $f_O = 0.58$, $f_H = -0.38$, and $f_D = 0.65$.

Then:[6]

$$F_{hkl} = f_{Ni} + 2f_O \cos 2\pi \left(\frac{2h + k}{3} + 0.25\ell\right) + 2 \times f_{H,D}$$

$$\cos 2\pi \left(\frac{2h + k}{3} + 0.46\ell\right)$$

The quantity x corresponds to the occupancy of the hydrogen sites and was taken as 1 for $Ni(OH)_2$ and 1/2 for NiOOH.

** This peak will be masked by nickel; the other will not.

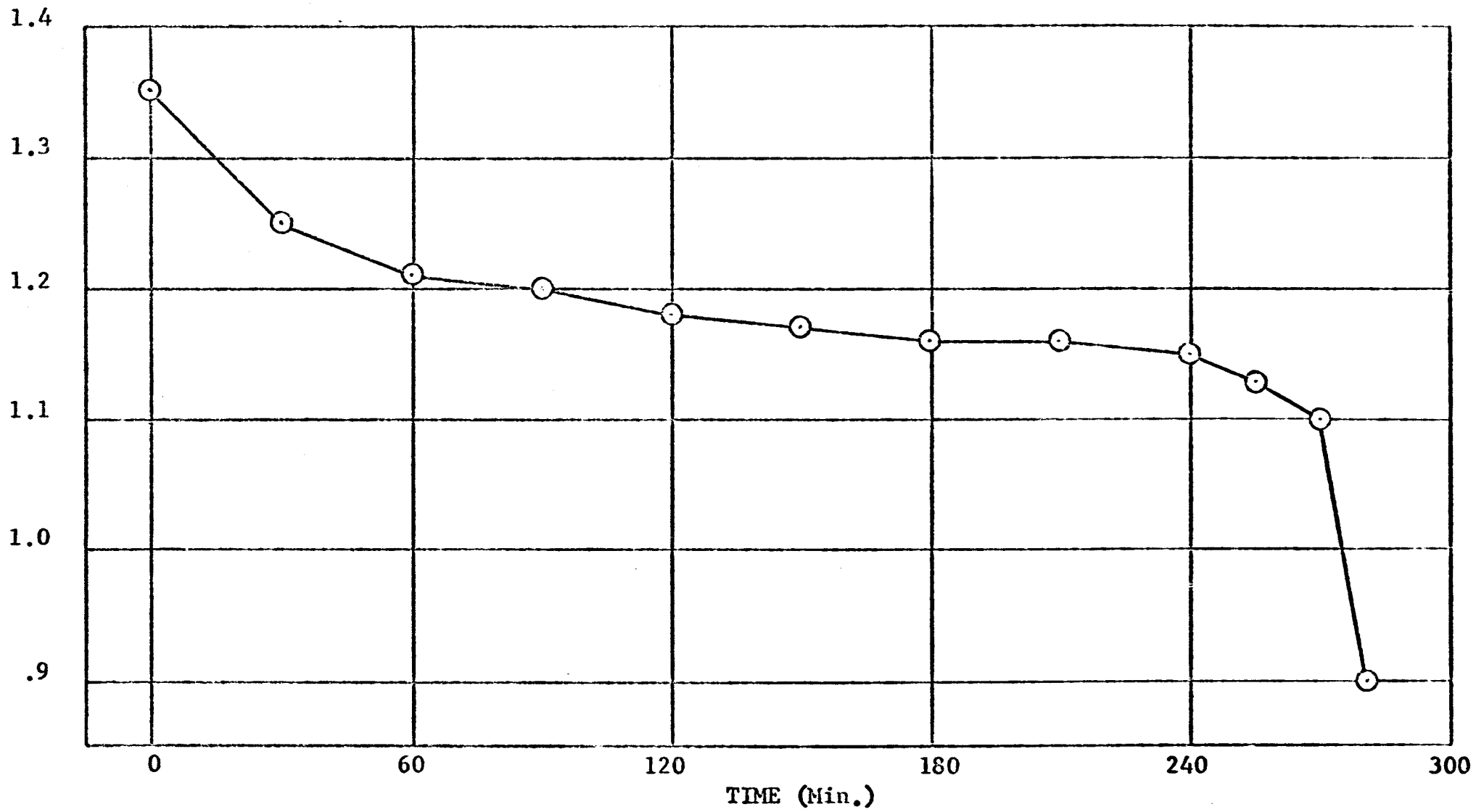

FIGURE 1. TYPICAL FORMATION DISCHARGE CURVE
CONTROL CELL

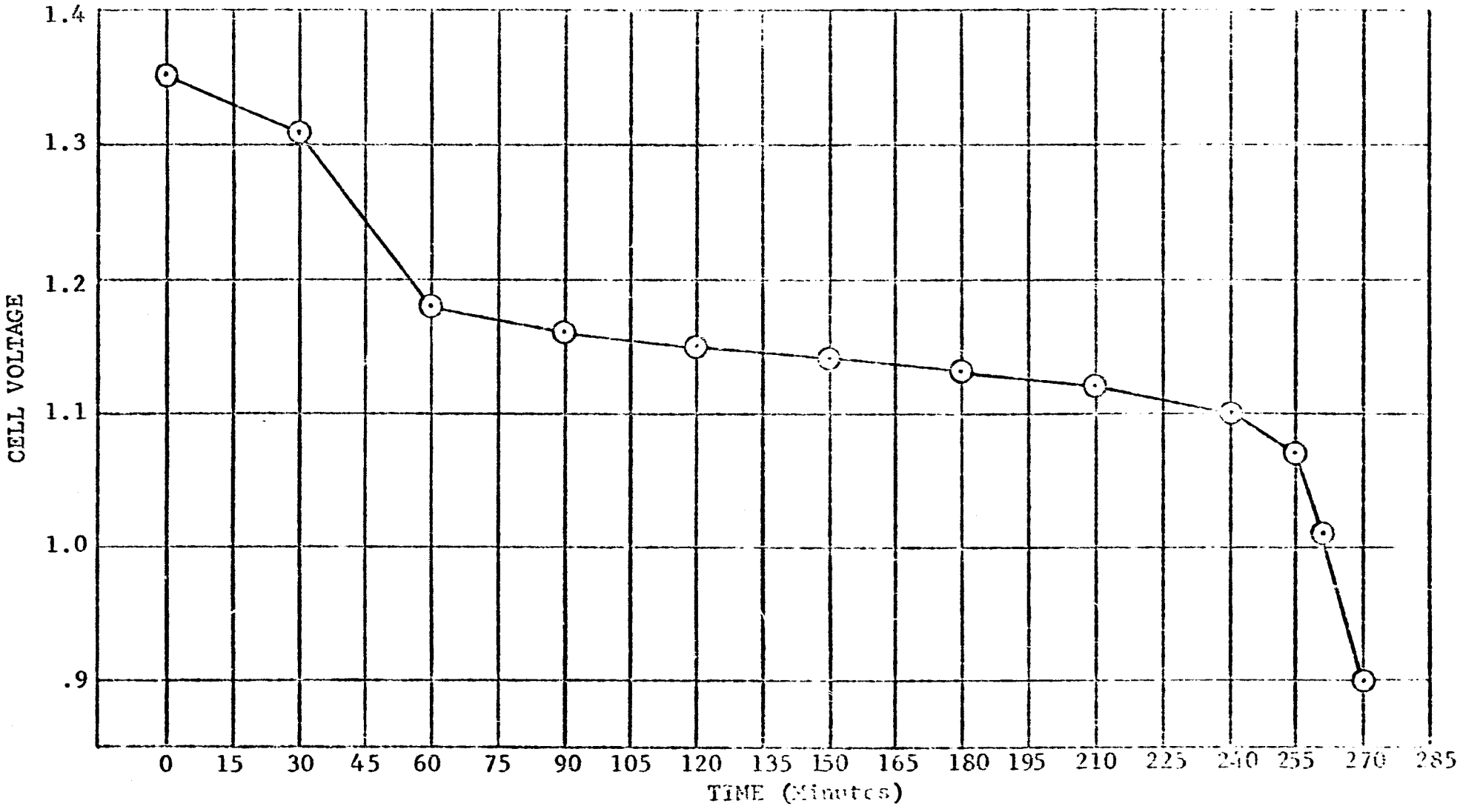

FIGURE 2 20% COBALT - TYPICAL FORMATION DISCHARGE, C/5 (200 mA)

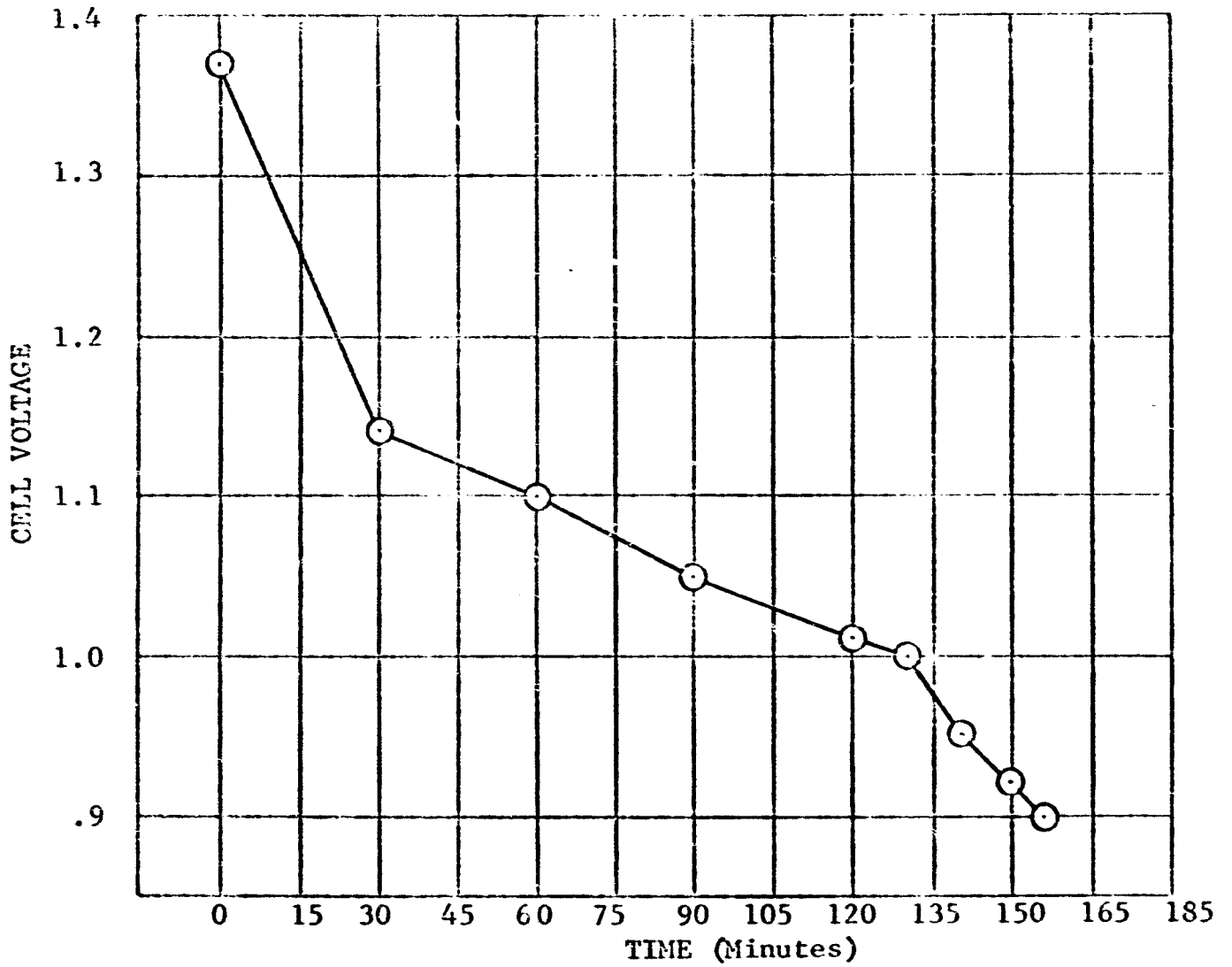

FIGURE 3. 40% COBALT - TYPICAL FORMATION DISCHARGE
C/5 (200 mA)

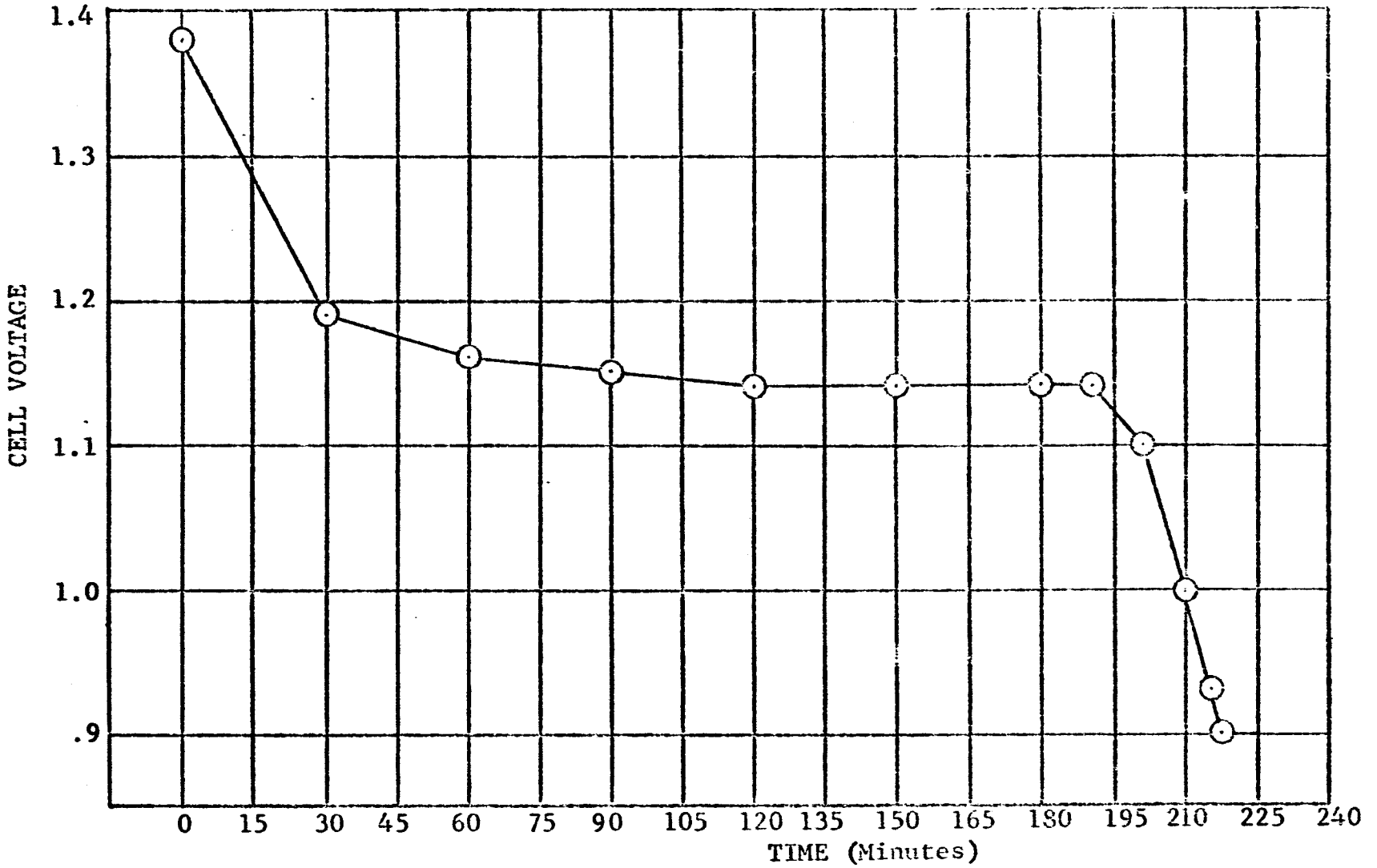

FIGURE 4 20% MANGANESE - TYPICAL FORMATION DISCHARGE, C/5 (200 mA)

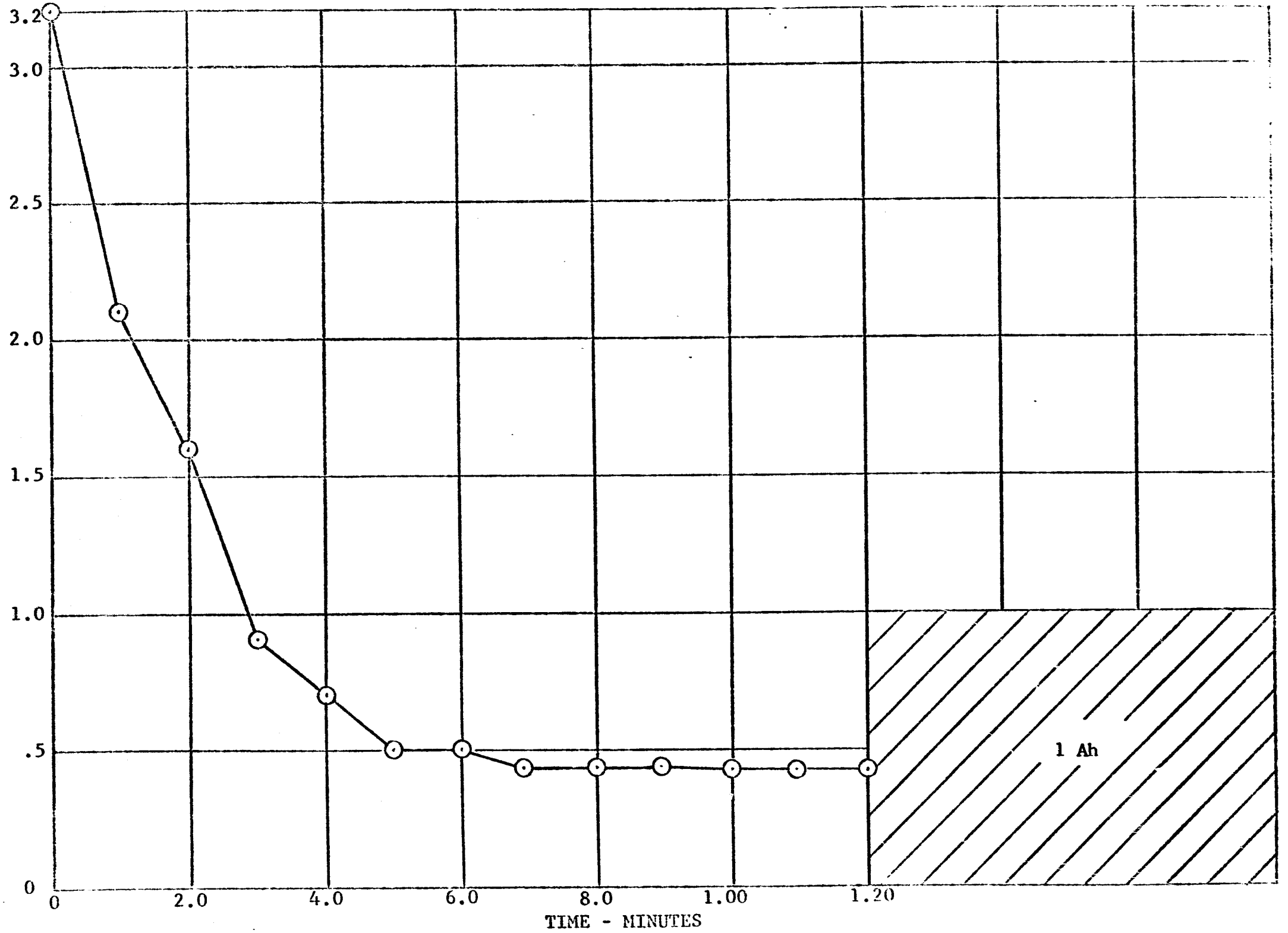

FIGURE 5 DETERMINATION OF AMPERE-HOUR INPUT ON CONSTANT VOLTAGE CHARGE OF 1.6 V/CELL FOR 2 HOURS

4-1684

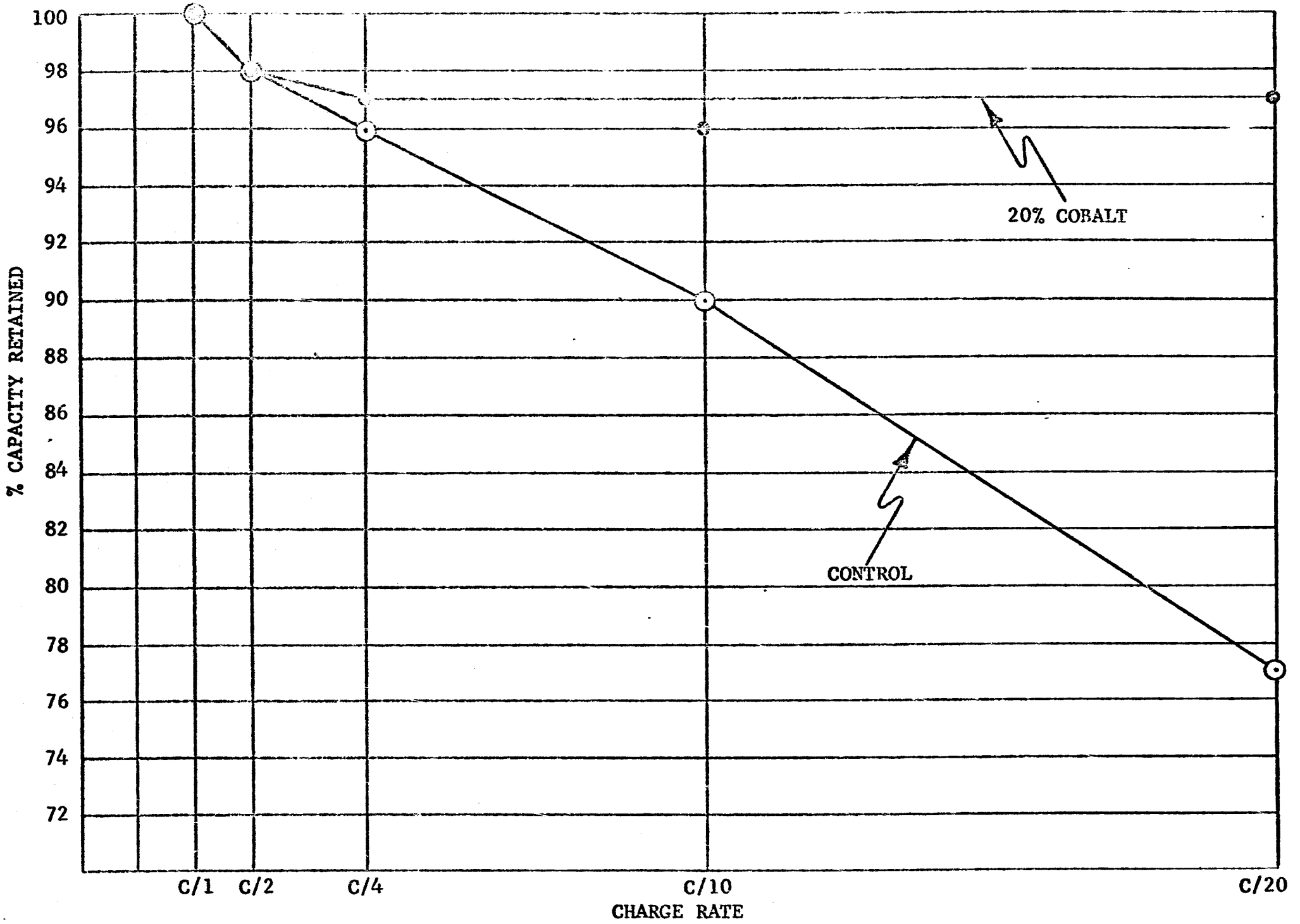

FIGURE 6 CHARGE ACCEPTANCE

4-1929

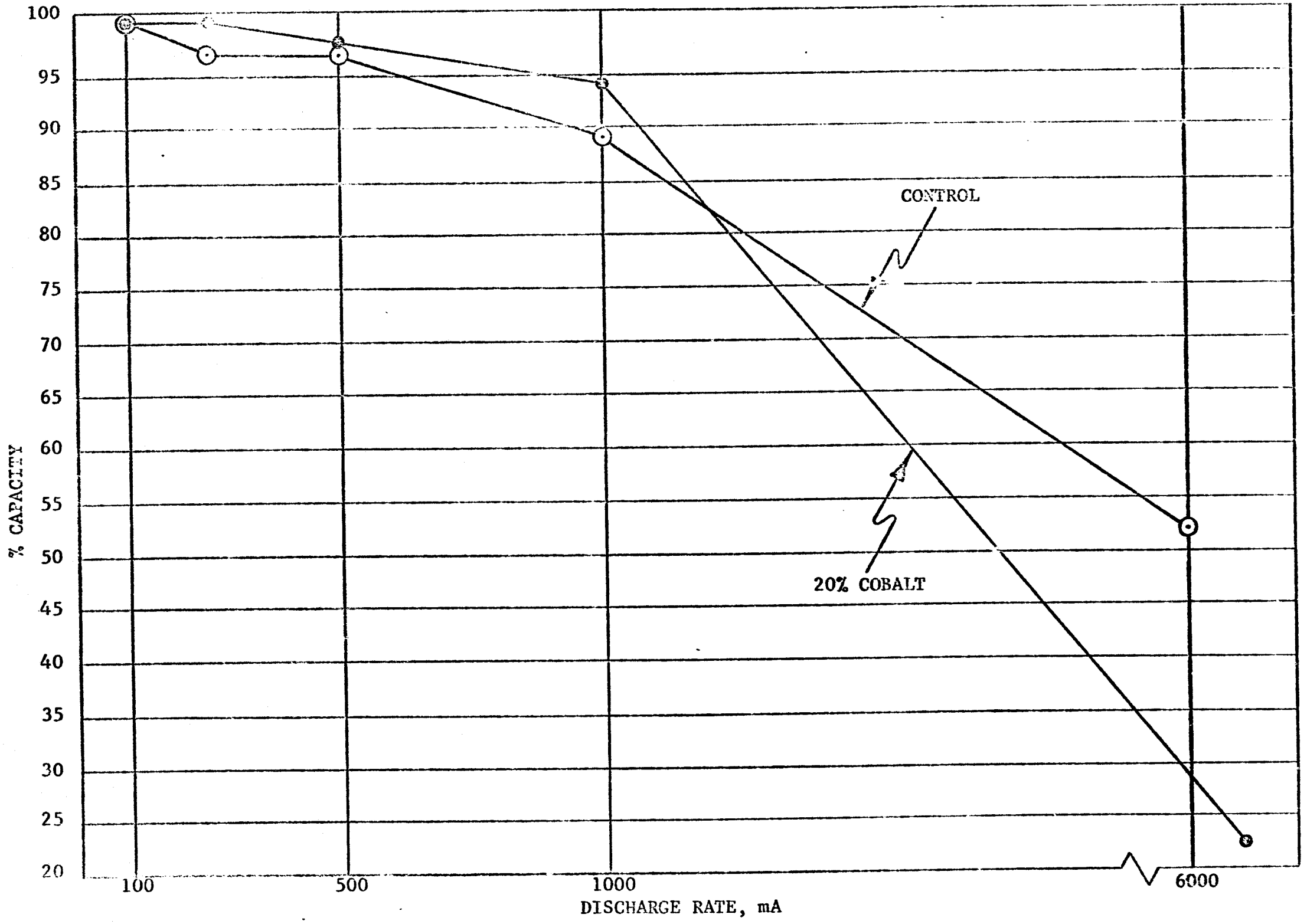

FIGURE 7 UTILIZATION AT VARIOUS RATES - DISCHARGED TO 0.9 V

4-1928

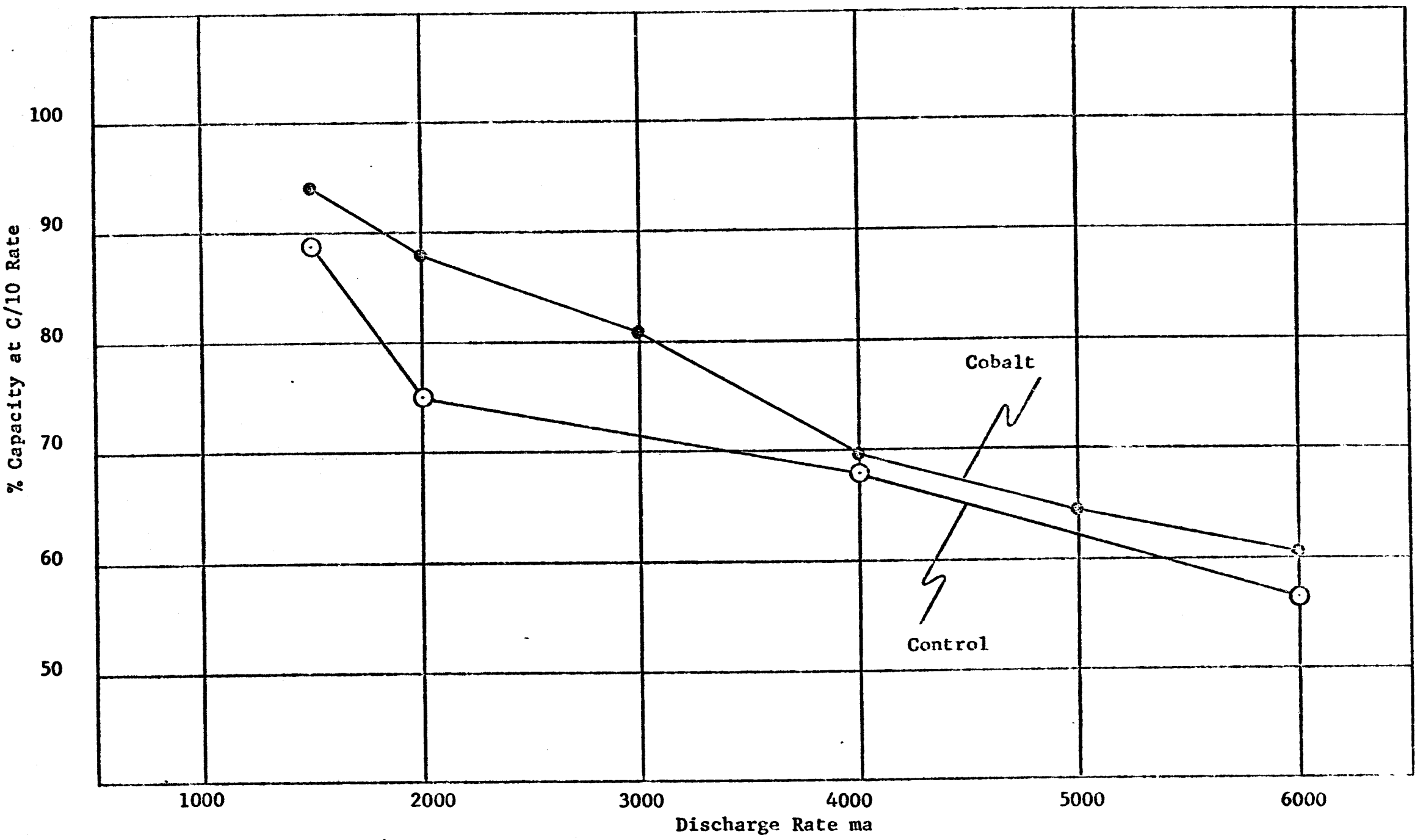

Figure 8 UTILIZATION AT VARIOUS RATES DISCHARGED TO 0.6 V

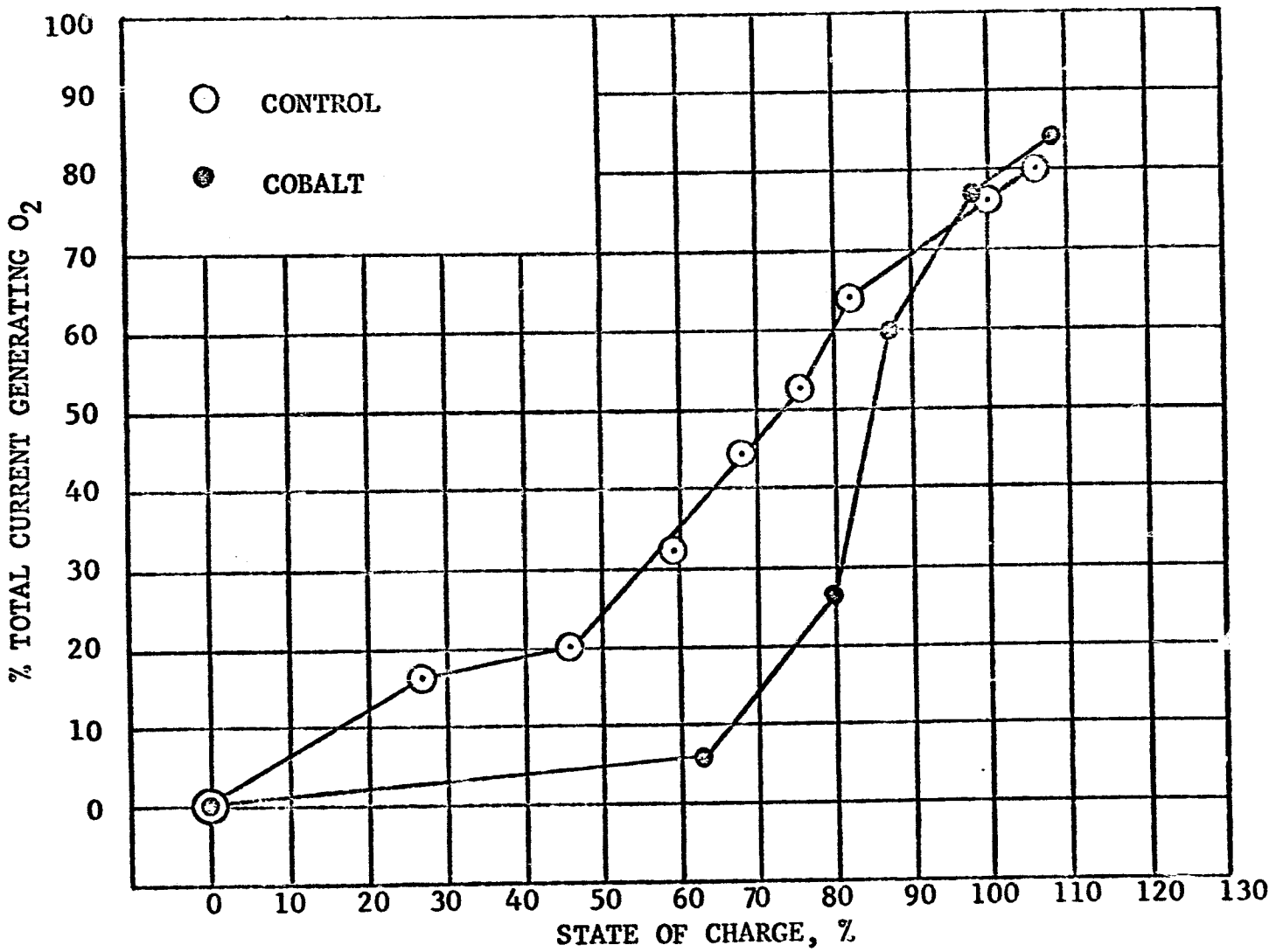

FIGURE 9 O_2 EVOLUTION, 100 mA

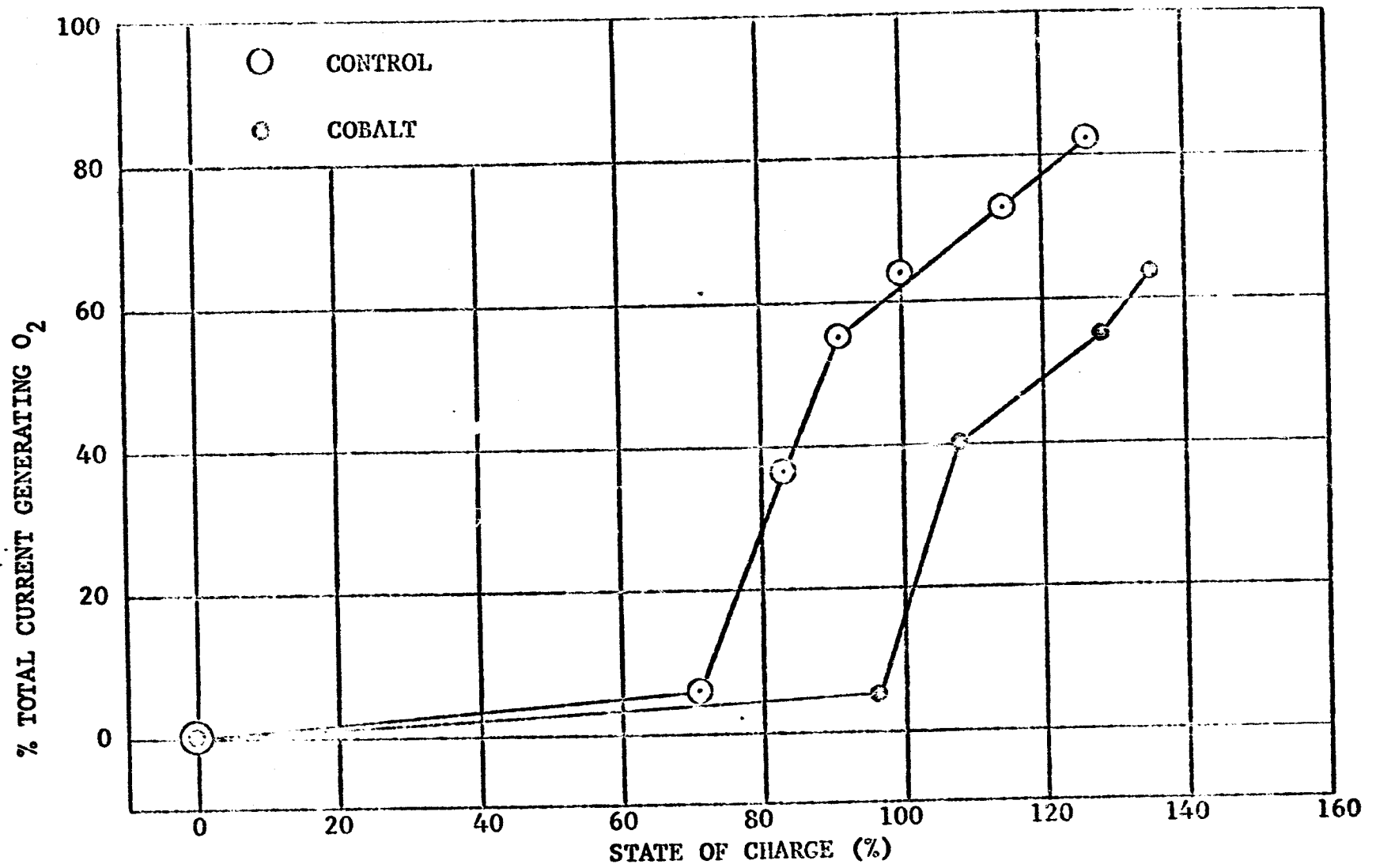

FIGURE 10 OXYGEN EVOLUTION -- I = 1/2 Ampere

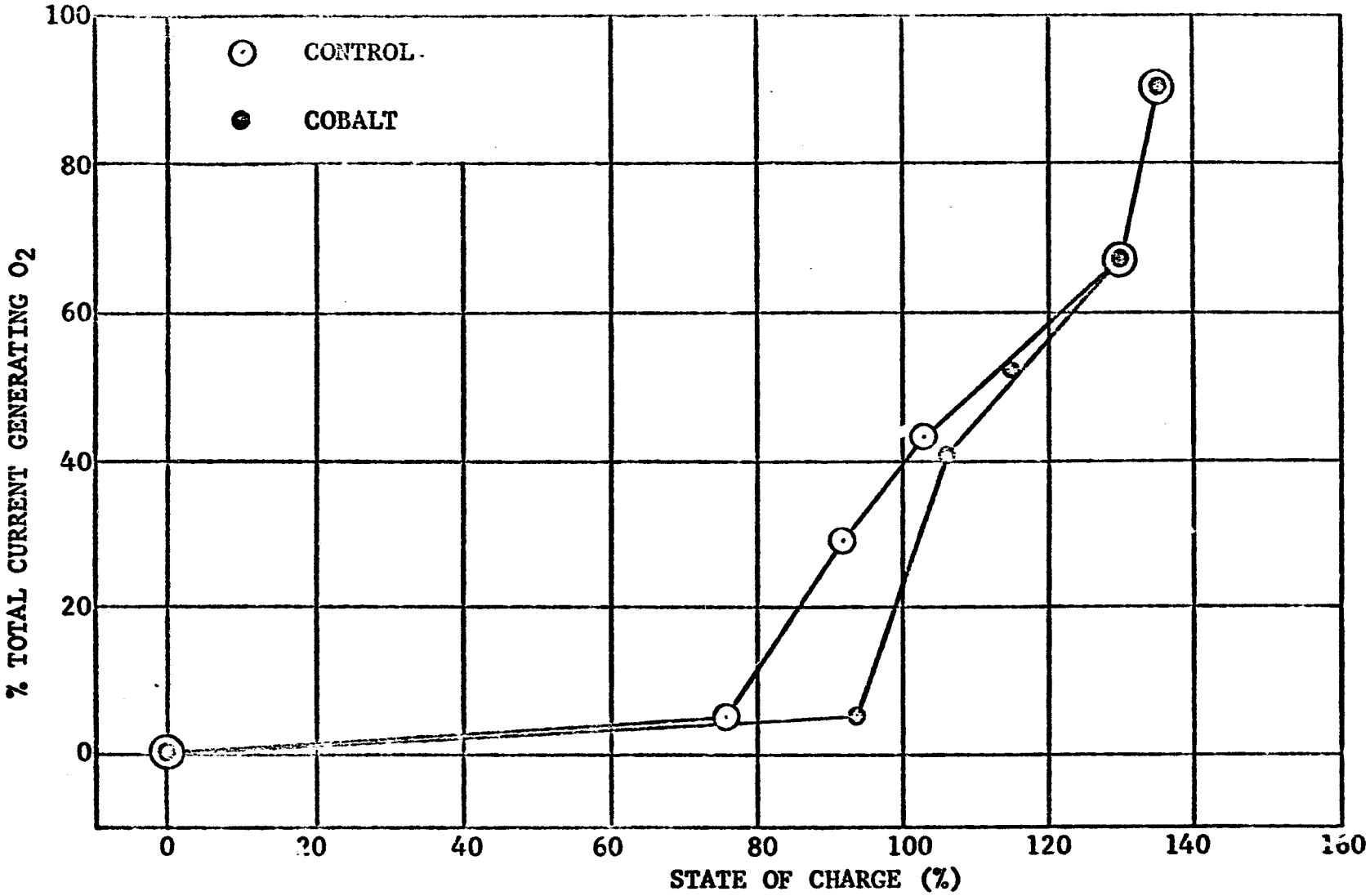

FIGURE 11 OXYGEN EVOLUTION -- I = 1 Ampere

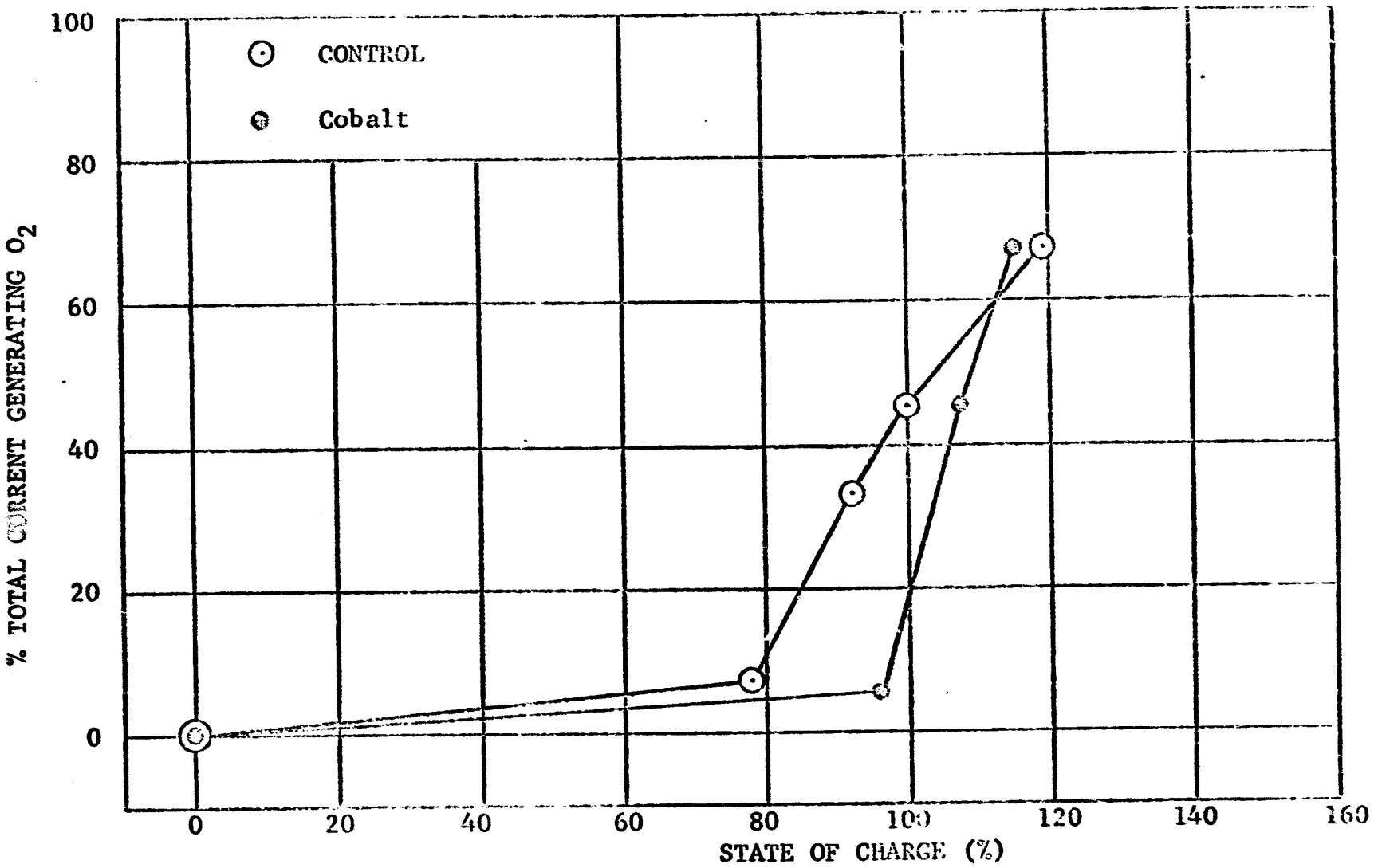

FIGURE 17 OXYGEN EVOLUTION -- I = 2 AMPERES

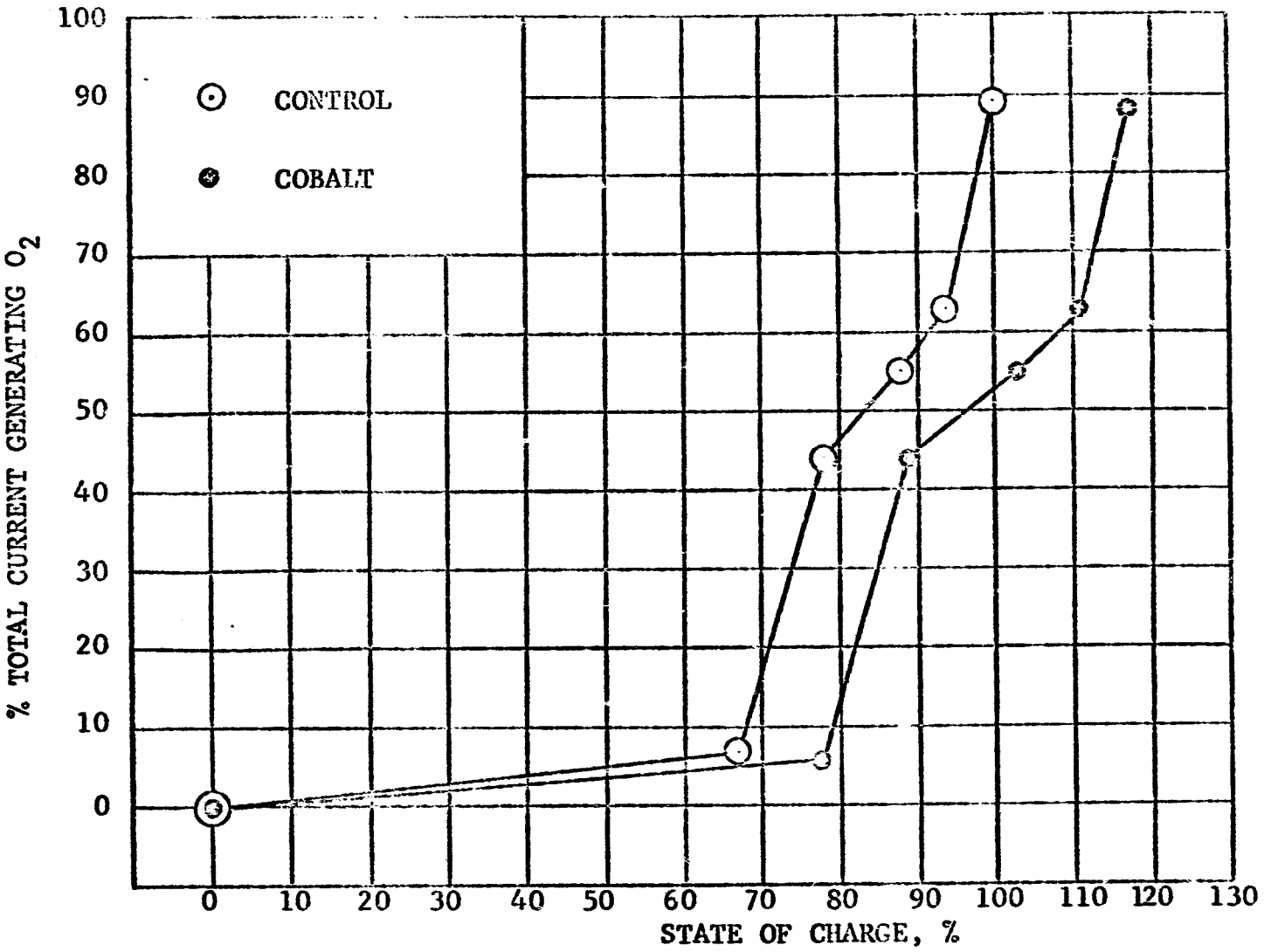

FIGURE 13 O_2 EVOLUTION, 6 AMPERES

FIG.14

X-RAY CURVE

TEST NO. _____ DATE _____
RADIATION Cu/Ni POWER 35 KVA 12 MA
SCALE 8 x 8 x 4 2θ/MIN 2
MATERIAL $Ni(OH)_2$
PHYSICAL STATE Electrode
HISTORY 50 Formed Discharged
COMMENTS

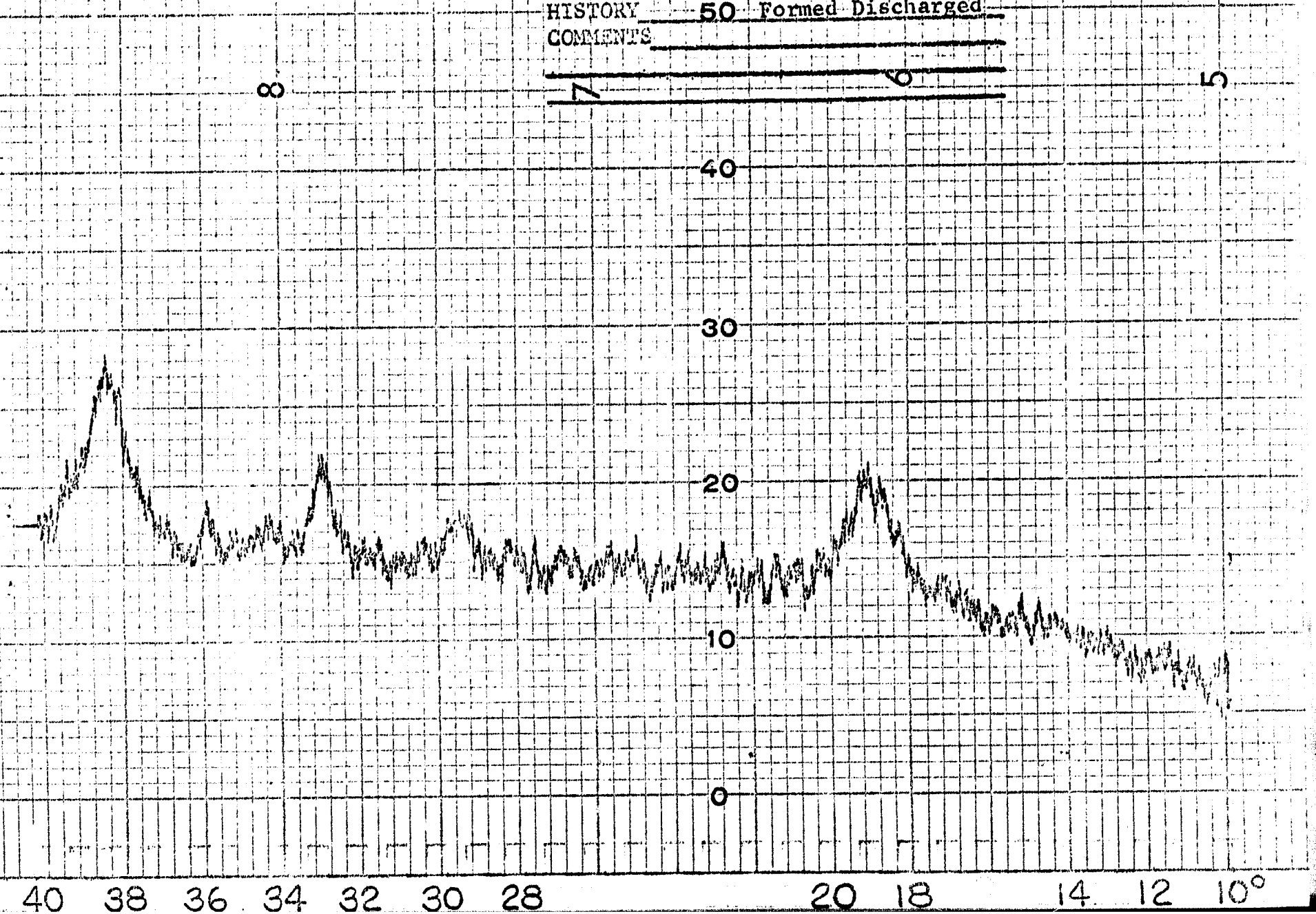

FIG. 15

X-RAY CURVE

TEST NO: DATE

RADIATION Cu Ni POWER 35 KVA 12 MA

SCALE 8 x 8 x 4 2θ/MIN 2

MATERIAL Ni(OH)$_2$

PHYSICAL STATE Electrode

HISTORY 90% Charged

COMMENTS

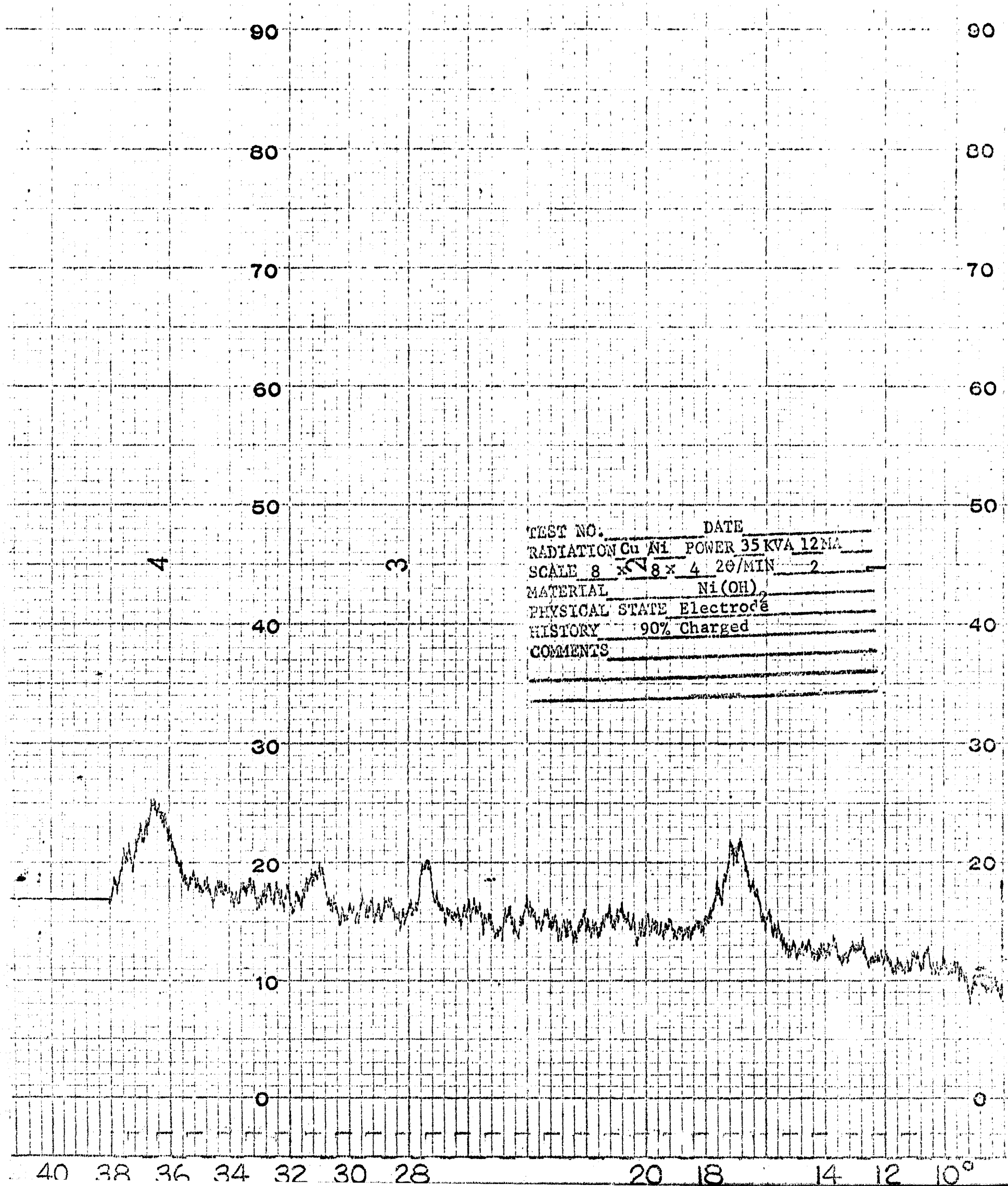

FIG. 16

X-RAY CURVE

90

80

70

60

50

40

30

20

10

0

11

10

9

TEST NO. DATE

RADIATION Cu/Ni POWER 35KVA 12MA

SCALE 8 x 8 x 4 2θ/MIN 2

MATERIAL $Ni(OH)_2$

PHYSICAL STATE Electrode

HISTORY 100% Charged

COMMENTS

40 38 36 34 32 30 28 20 18 14 12 10°

FIG. 17

X-RAY CURVE

TEST NO. 8 DATE

RADIATION Cu / Ni POWER 35 KVA 12MA

SCALE 8 x 8 x 4 2θ/MIN 2

MATERIAL $Ni(OH)_2$

PHYSICAL STATE Positive Electrode

HISTORY 150% Charged

COMMENTS

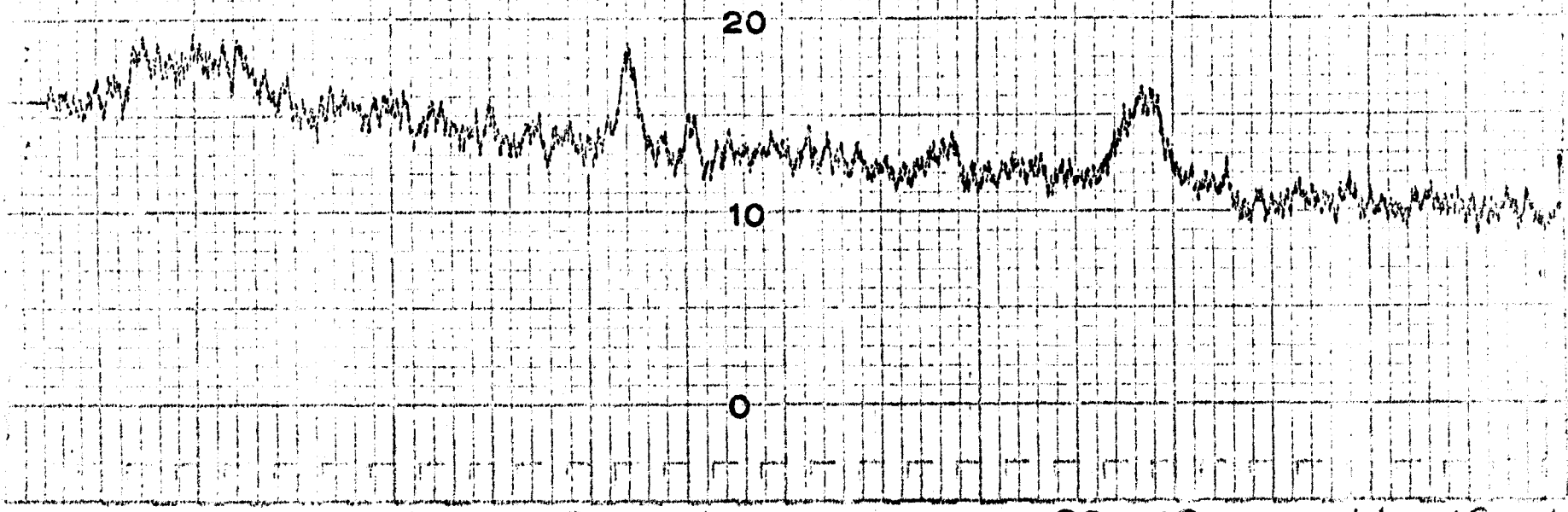

FIG.18
X-RAY CURVE

TEST NO._____ DATE_____
RADIATION Cu/Ni POWER 35 KVA 12 MA
SCALE 8 x 8 x 4 20/MIN 2
MATERIAL Ni(OH)$_2$
PHYSICAL STATE Positive Electrode
HISTORY Charged 200%
COMMENTS_____

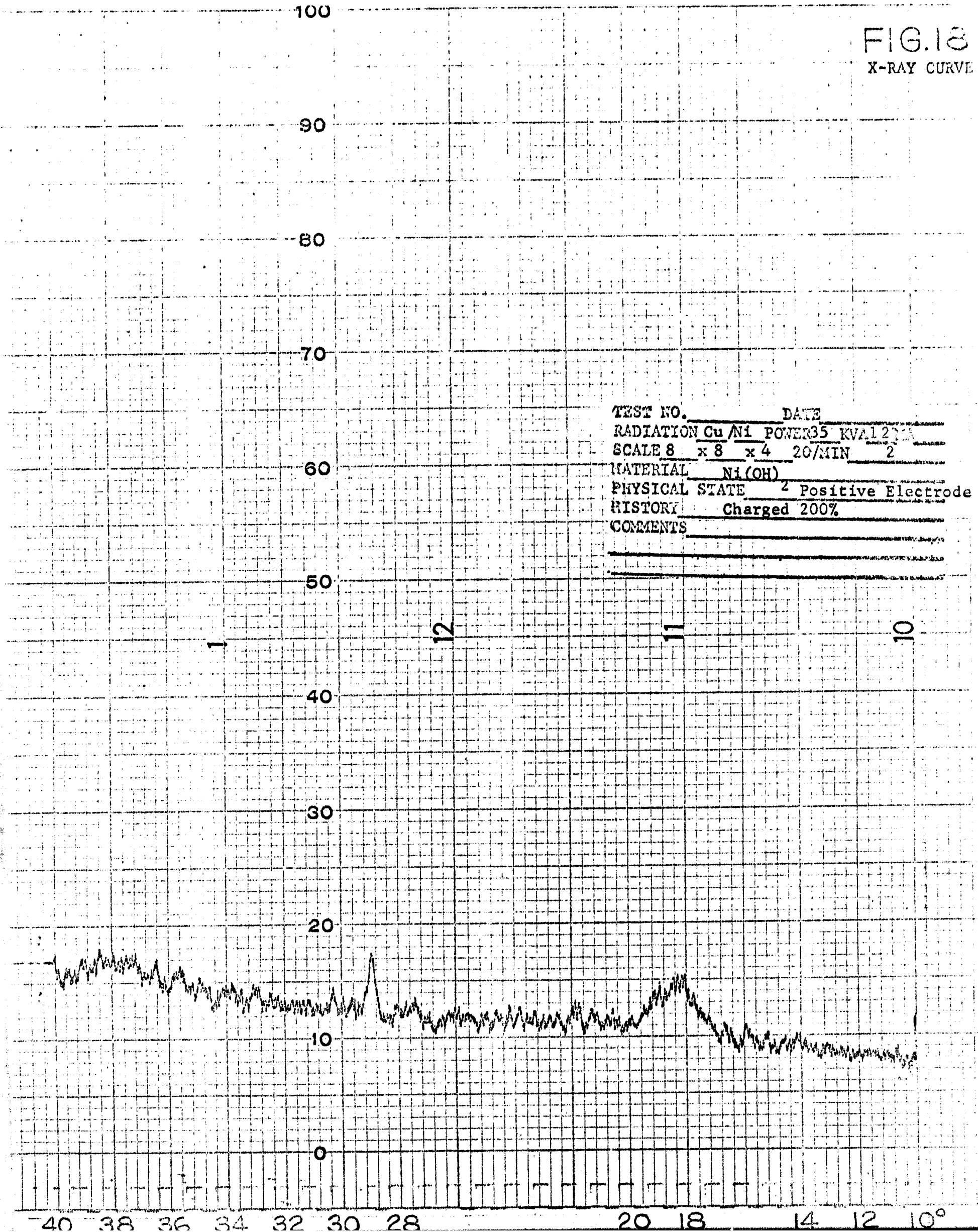

FIG. 19

X-RAY CURVE

TEST NO. _____ DATE _____

RADIATION Cu / Ni POWER 35 KVA 12 MA

SCALE 8 × 8 × 4 2θ/MIN 2

MATERIAL $Ni(OH)_2$

PHYSICAL STATE Electrode

HISTORY 600% Charged

COMMENTS _____

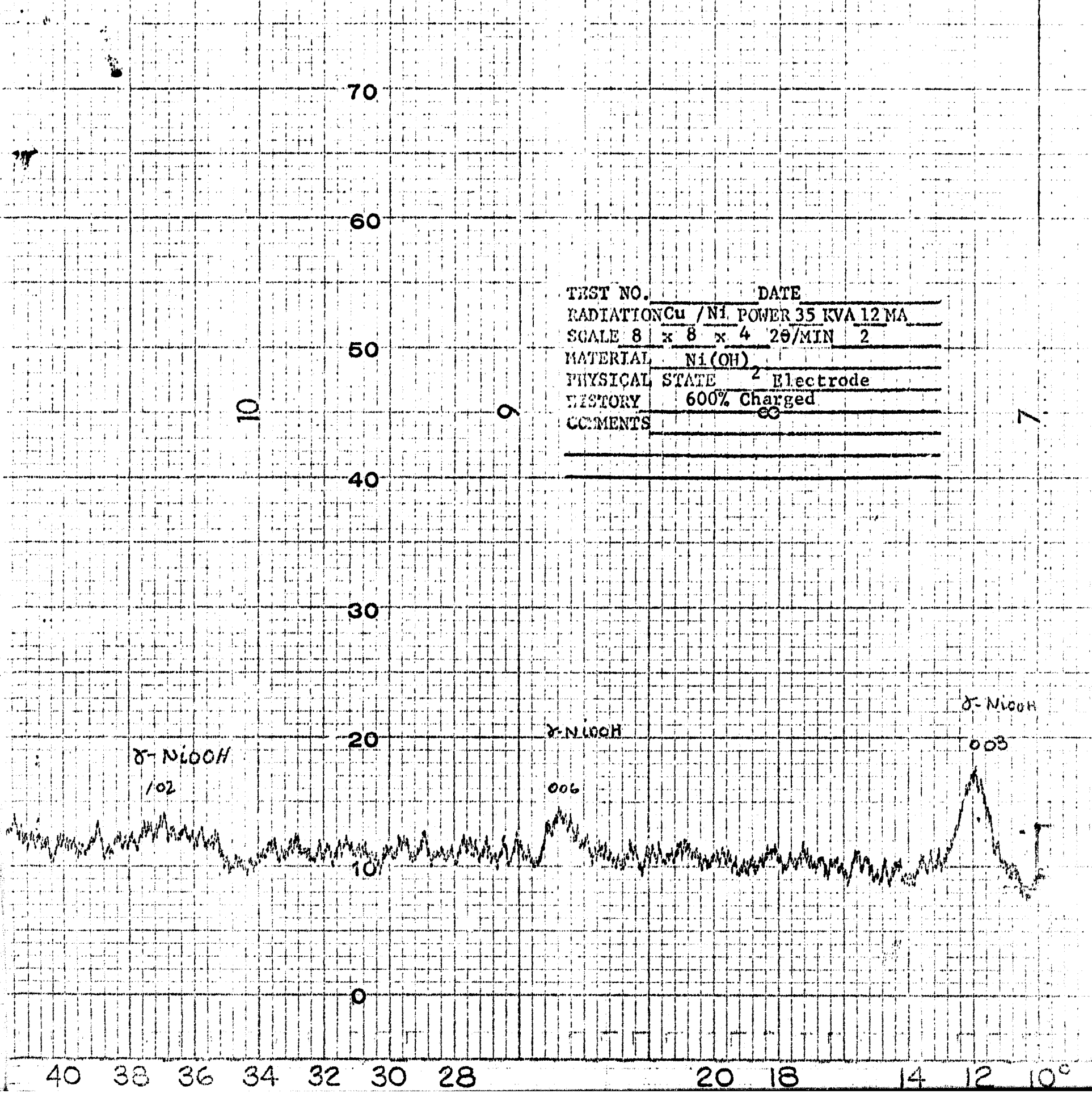

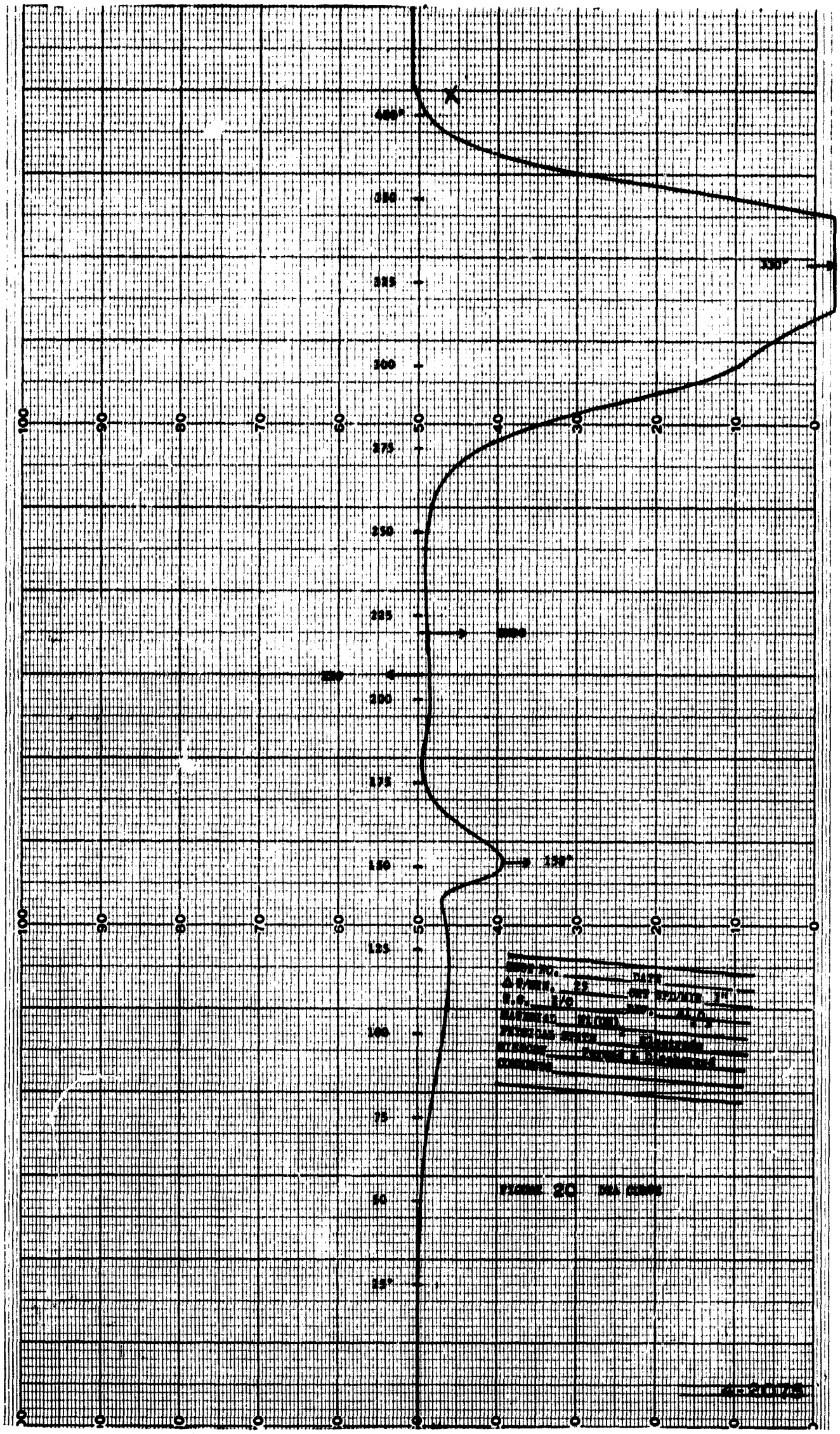

FIGURE 20 DSA CURVE

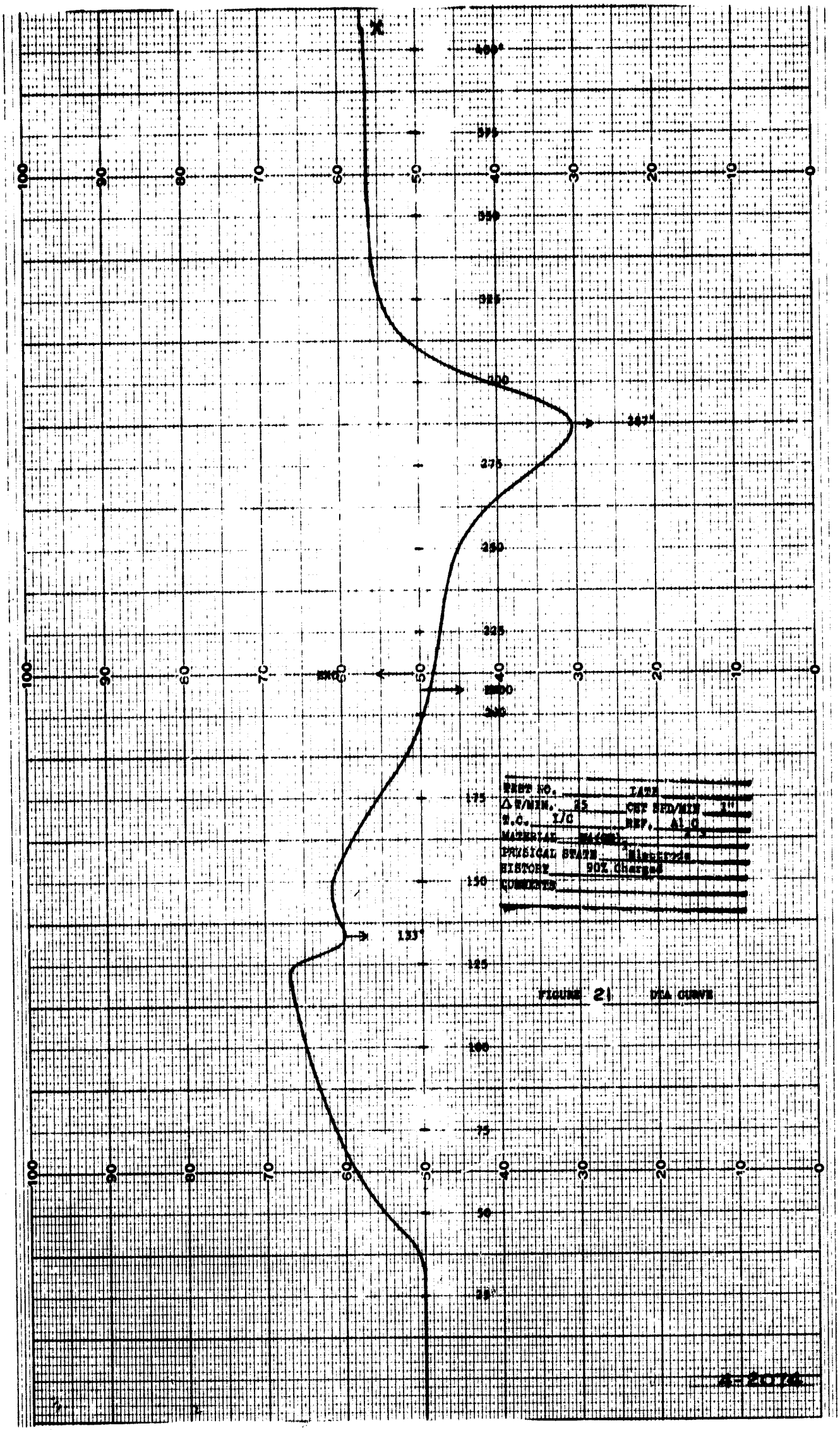
X
100
90
80
70
60
50
40
30
20
10
0
350
325
300
275
250
225
200
175
150
125
100
75
50
25
133°
TEST NO.
ΔT/MIN. 25
S.C. I/C
MATERIAL
PHYSICAL STATE
HISTORY 90% Charged
COMMENTS
DTA CURVE
S-2014

FIGURE 21

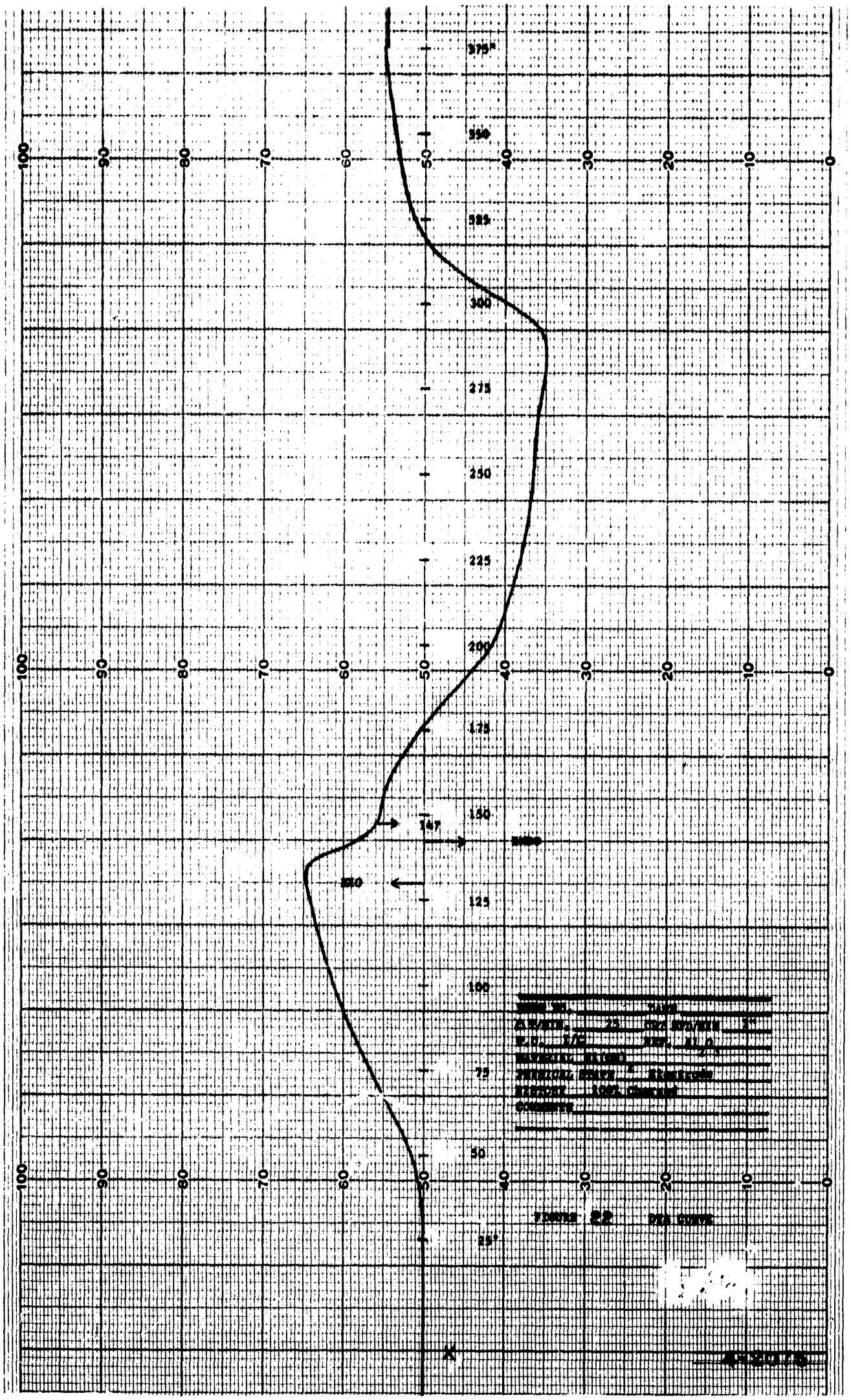
375°
350
325
300
275
250
225
200
175
150
125
100
75
50
25°
147
150
125
100
75
50
25°
100
90
80
70
60
50
40
30
20
10
0

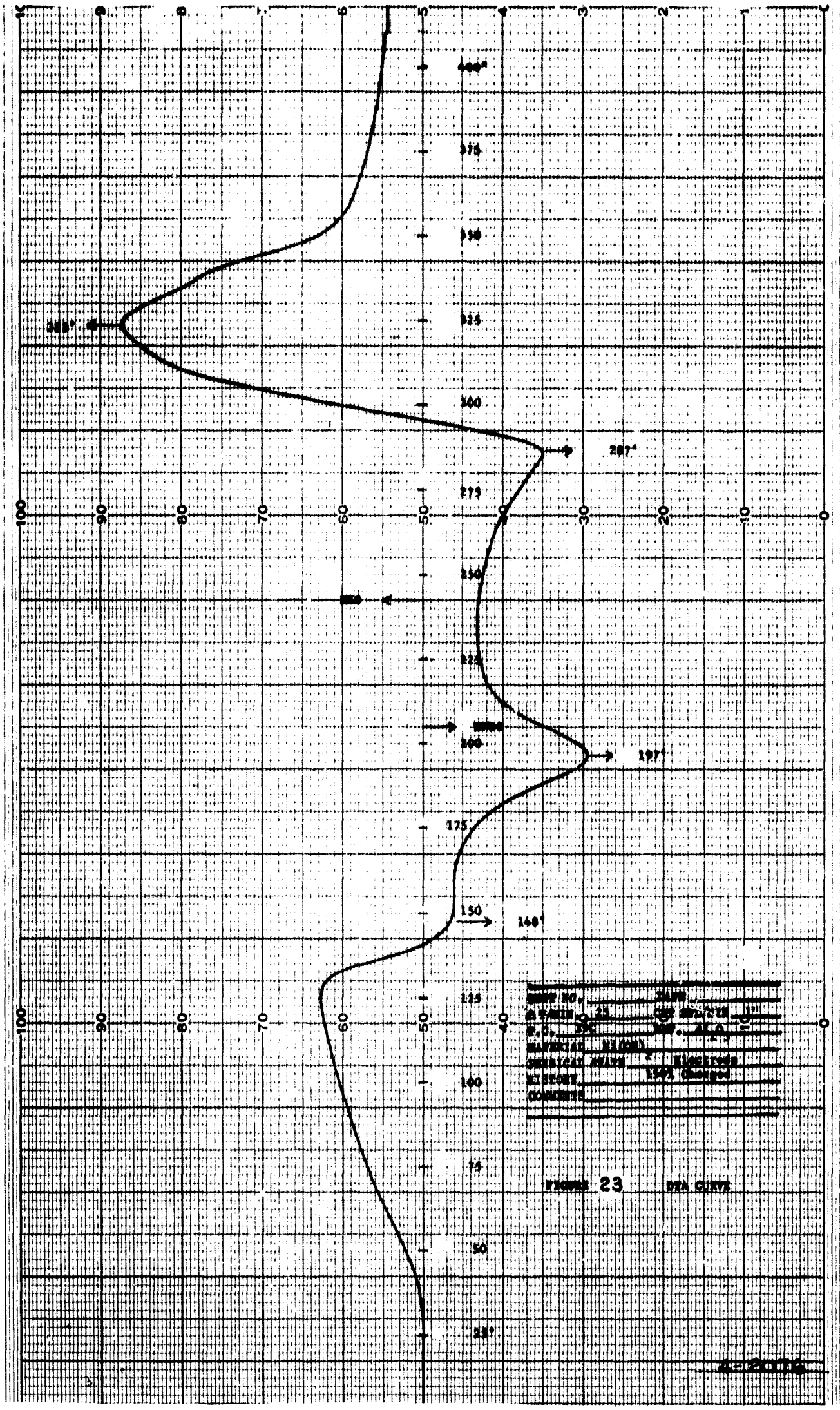

FIGURE 23 DTA CURVE

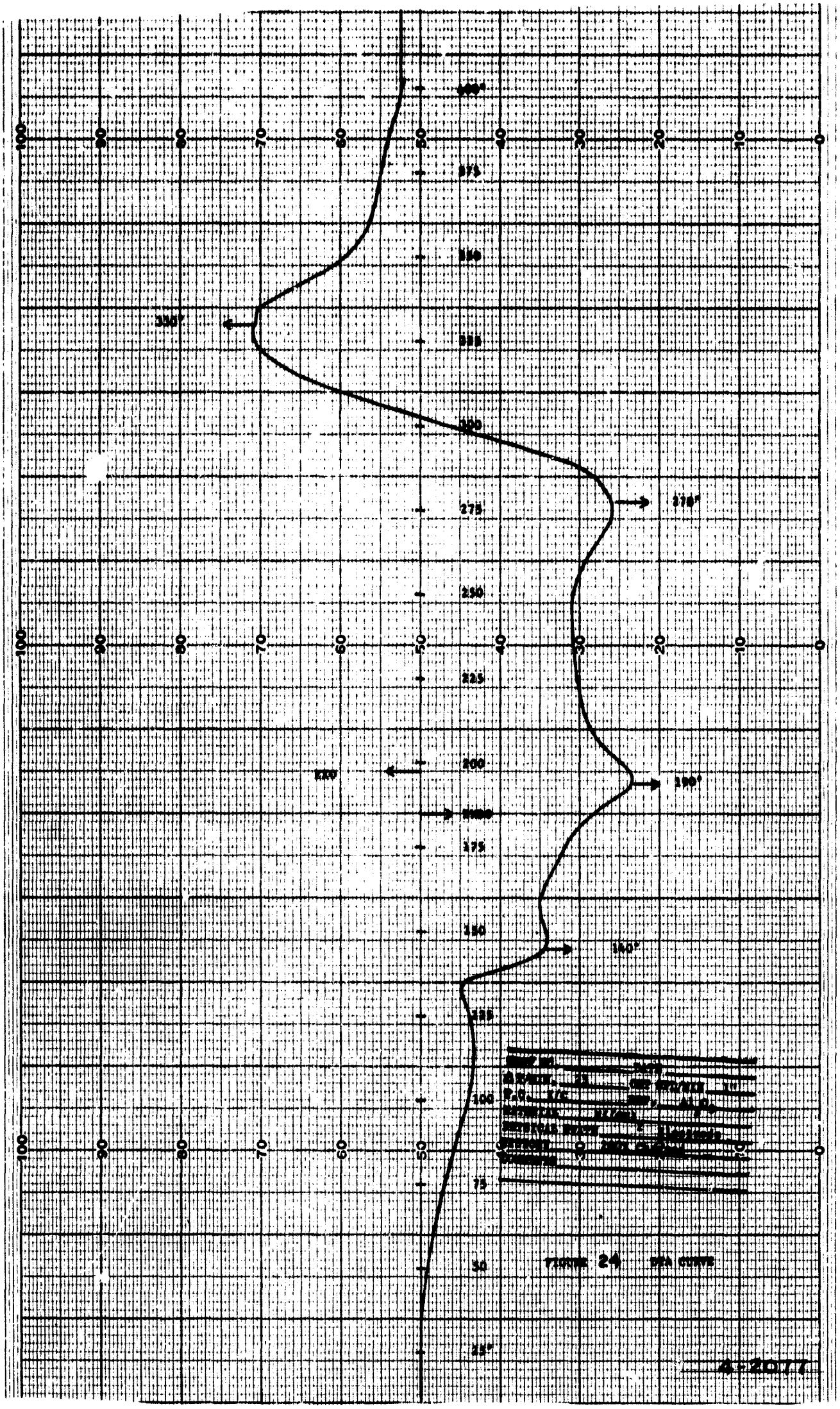
100
90
80
70
60
50
40
30
20
10
0
350
325
300
275
250
225
200
175
150
125
100
75
50
25
330°
270°
190°
140°
120
FIGURE 24 DRA CURVE
4-20-77

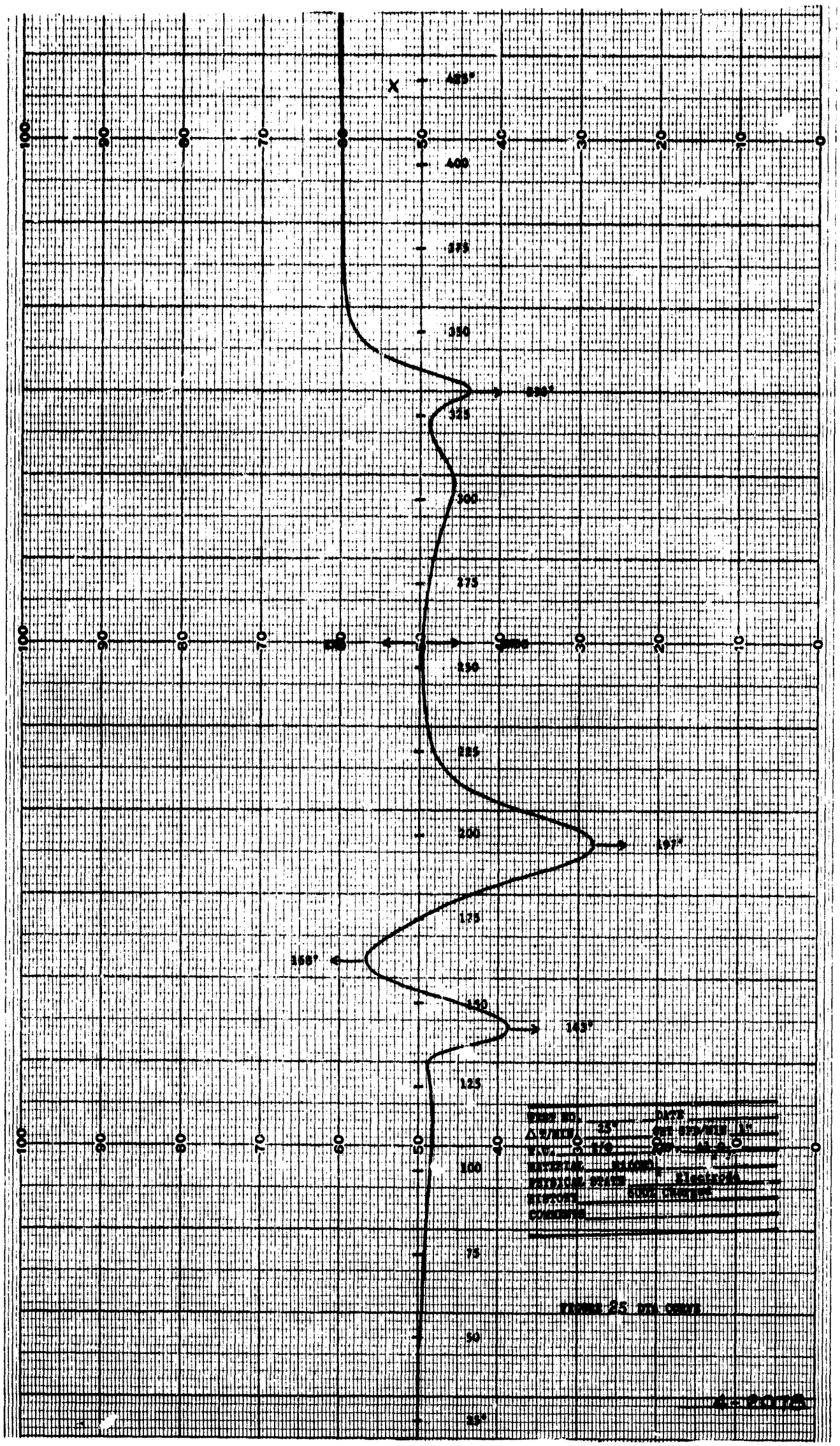
X
425°
400
375
350
325°
300
275
250
225
200
197°
175
168°
150
143°
125
100
75
50
25°
100
90
80
70
60
50
40
30
20
10
0

FIG. 26

X-RAY CURVE

TEST NO. _____ DATE _____
RADIATION Cu/Ni POWER 35 KVA 12 M.A.
SCALE 8 x 8 x 4 2θ/MIN 2
MATERIAL 20% Cobalt
PHYSICAL STATE Electrode
HISTORY Formed Discharged
COMMENTS _____

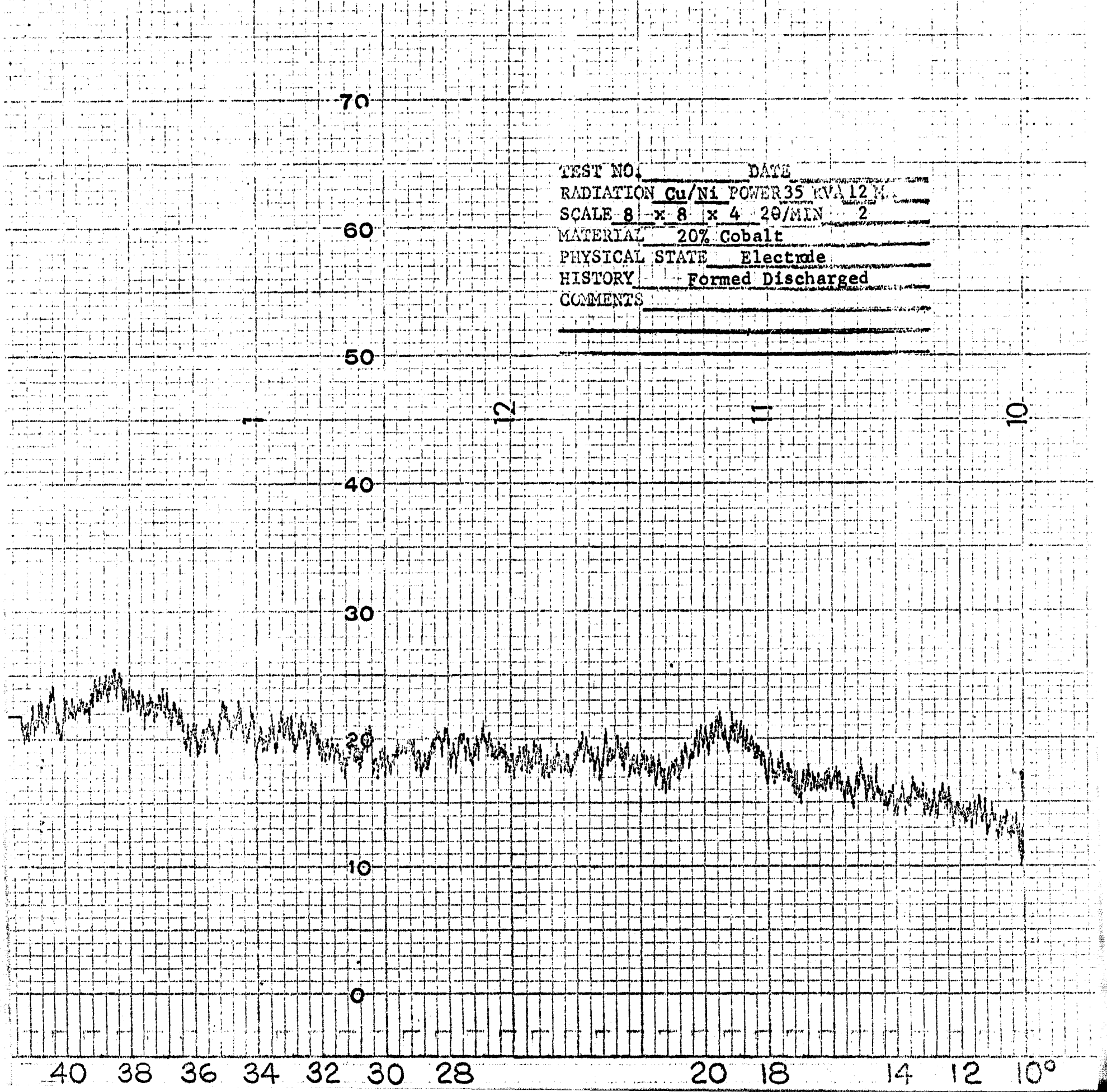

FIG. 27

X-RAY CURVE

TEST NO. _____ DATE _____
RADIATION Cu/Ni POWER 35 KVA 12 MA
SCALE 8 x 8 x 4 2° /MIN 2
MATERIAL 20% Cobalt
PHYSICAL STATE Electrode
HISTORY 90% Charged
COMMENTS _____

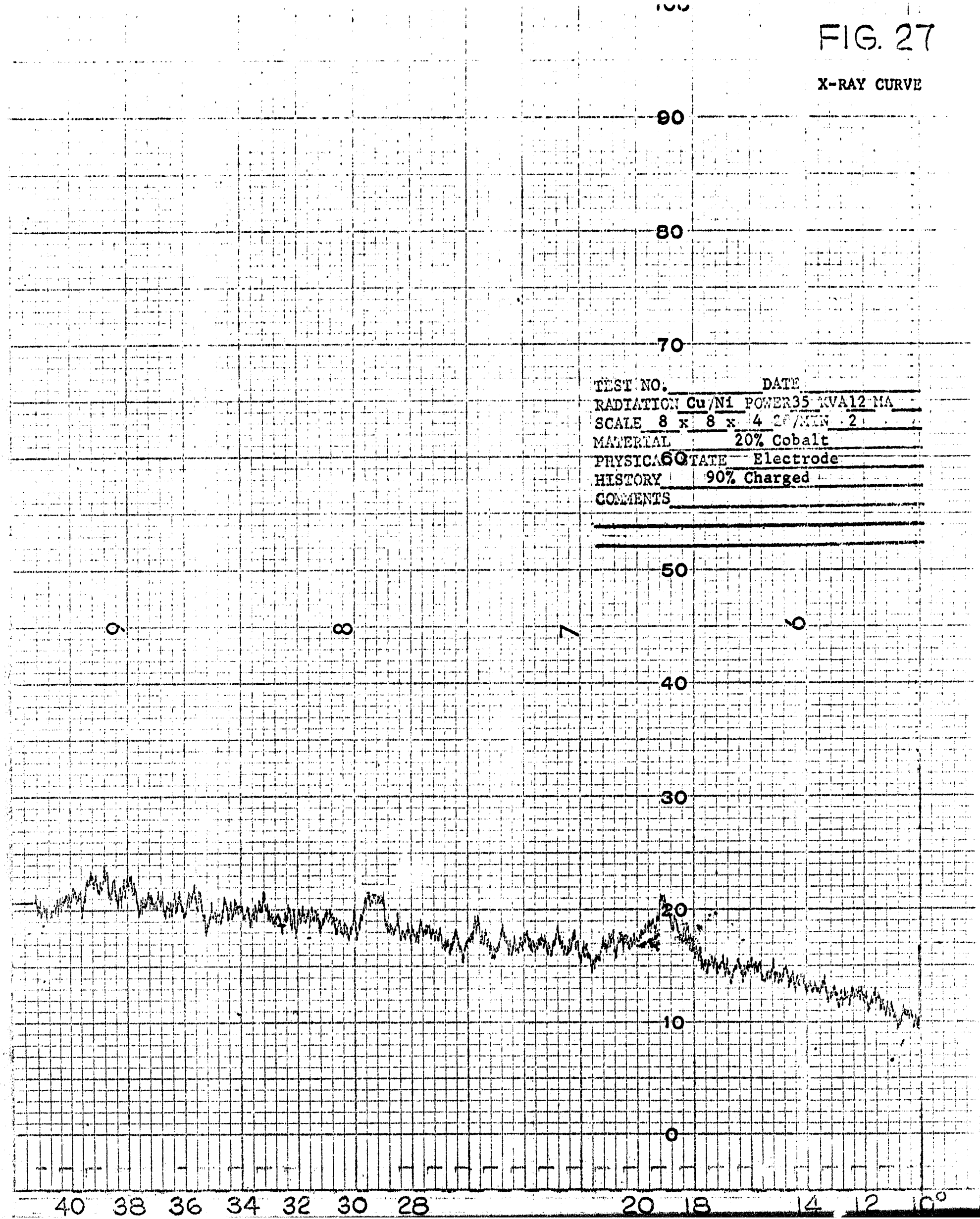

FIG. 28

X-RAY CURVE

TEST NO. _____ DATE _____
RADIATION Cu / Ni POWER 35 KVA 12 MA
SCALE 8 x 8 x 4 2θ/MIN 2
MATERIAL 20% Cobalt
PHYSICAL STATE Electrode
HISTORY 100% Charged
COMMENTS

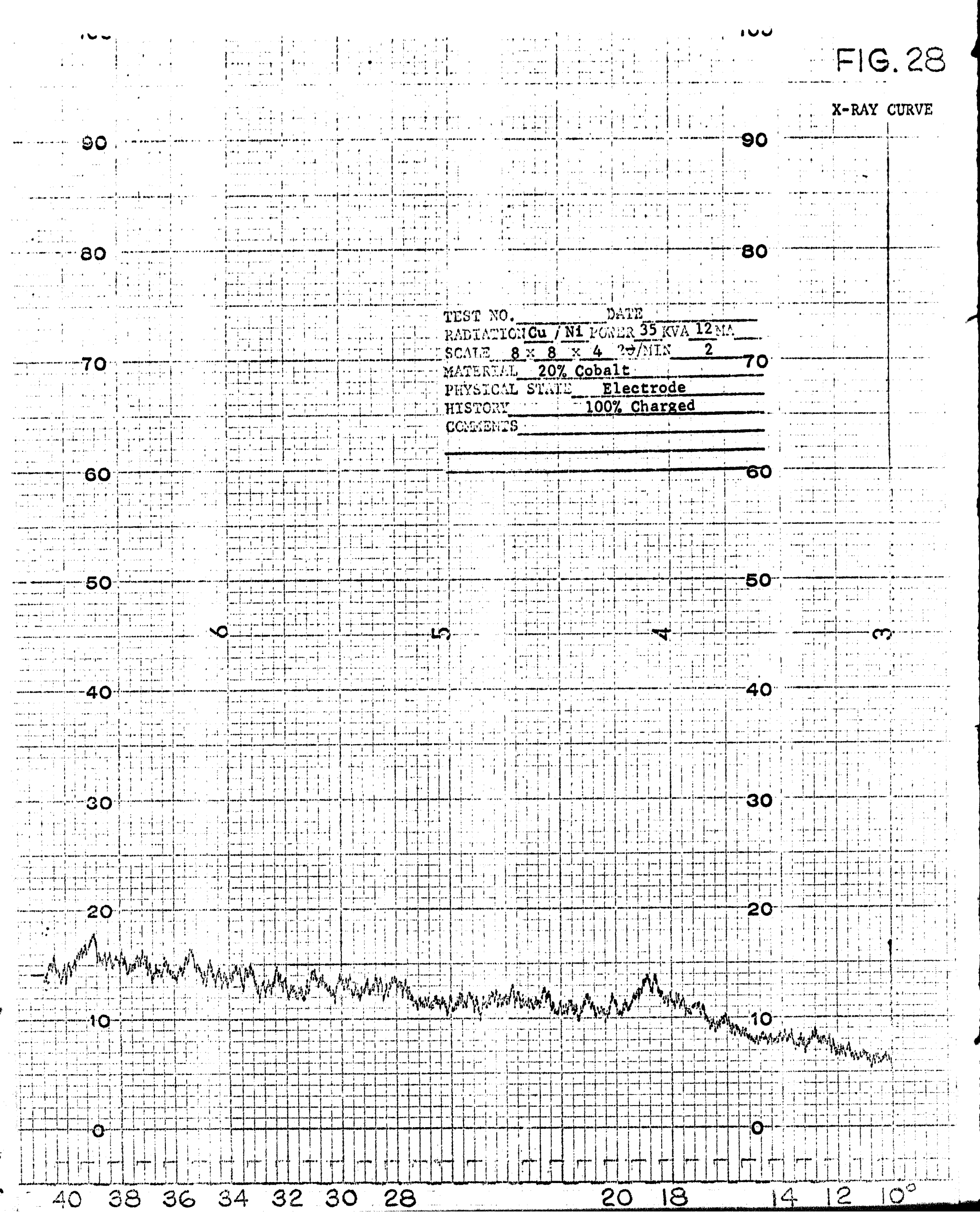

FIG. 29

X-RAY CURVE

TEST NO. 12 DATE 11

RADIATION Cu/Ni POWER 35 KVA 12 MA

SCALE 8 x 8 x 4 2θ/MIN 2

MATERIAL 20% Cobalt

PHYSICAL STATE Electrode

HISTORY 150% Charged

COMMENTS

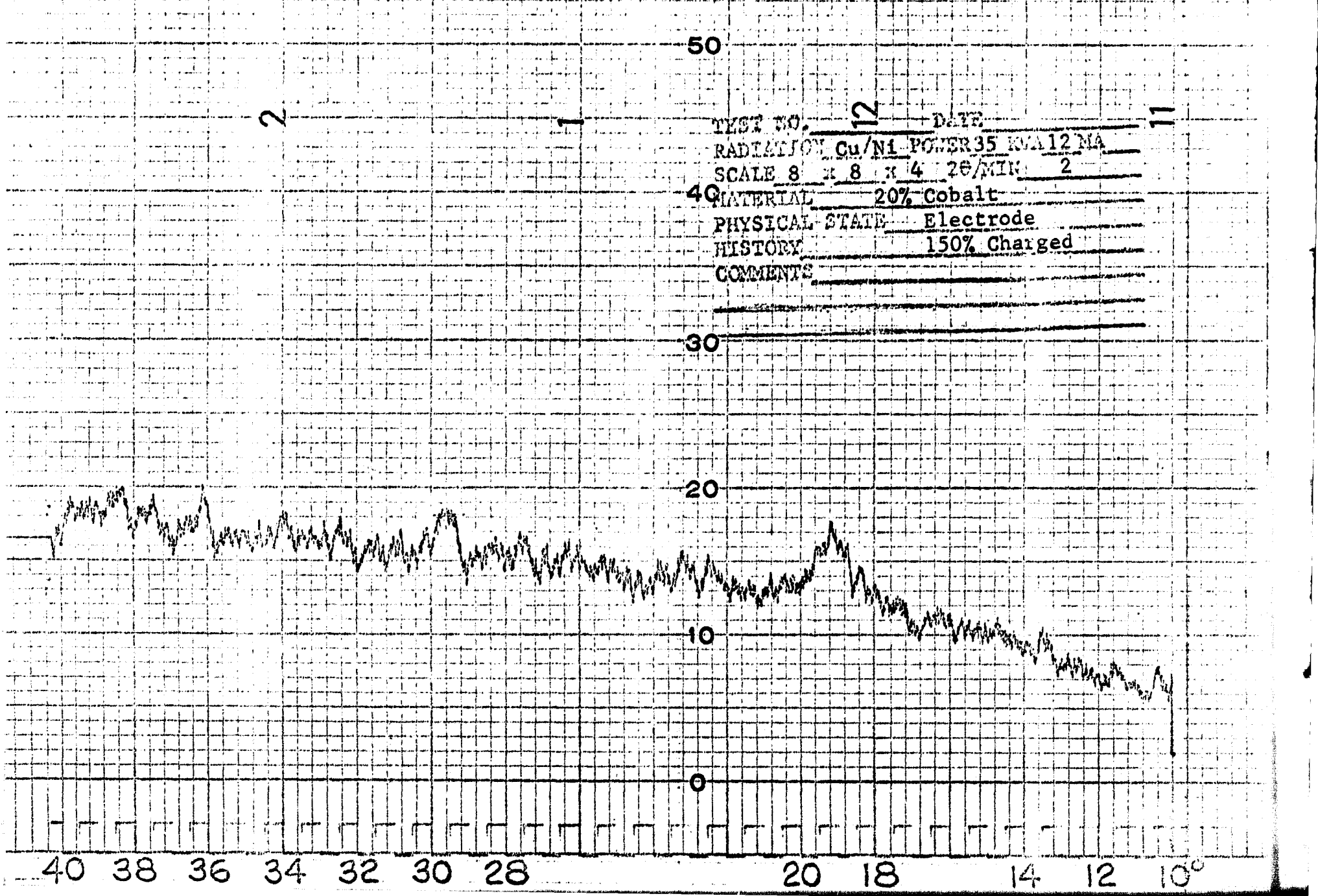

FIG. 30

X-RAY CURVE

TEST NO. DATE

RADIATION Cu / Ni POWER 35 KVA 12 MA

SCALE 8 x 8 x 4 2θ/MIN 2

MATERIAL 20% Cobalt

PHYSICAL STATE Positive Electrode

HISTORY 200% Charged

COMMENTS

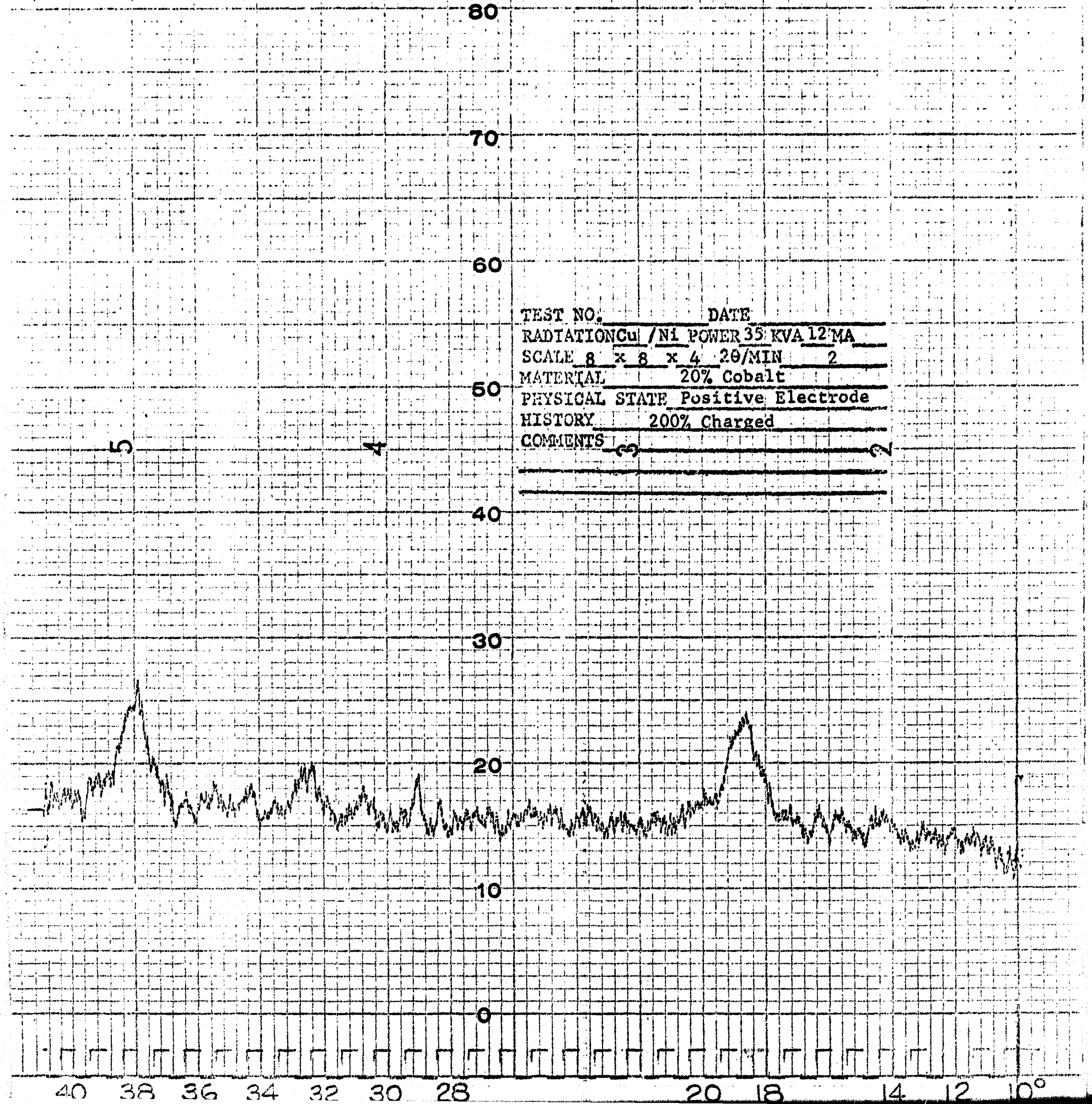

FIG. 31

X-RAY CURVE

TEST NO. _____ DATE _____

RADIATION Cu/Ni POWER 35KVA 12MA

SCALE 8 x 8 x 4 2θ/MIN 2

MATERIAL 20% Cobalt

PHYSICAL STATE Electrode

HISTORY 600% Charged

COMMENTS 2

Ni(OH)2

001

γ NiOOH

003

4 3

90 80 70 60 50 40 30 20 10 0

40 38 36 34 32 30 28 20 18 14 12 10°

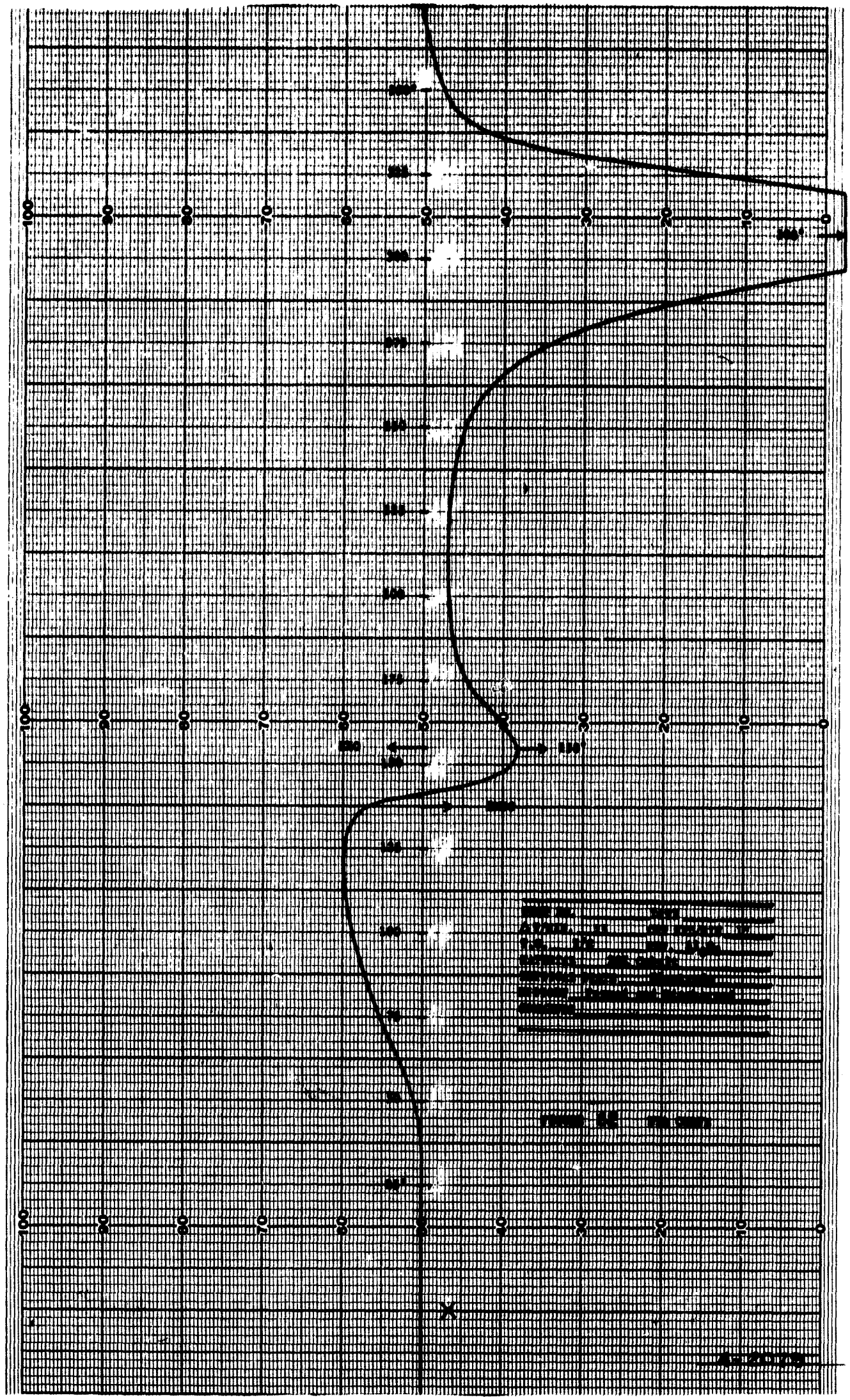

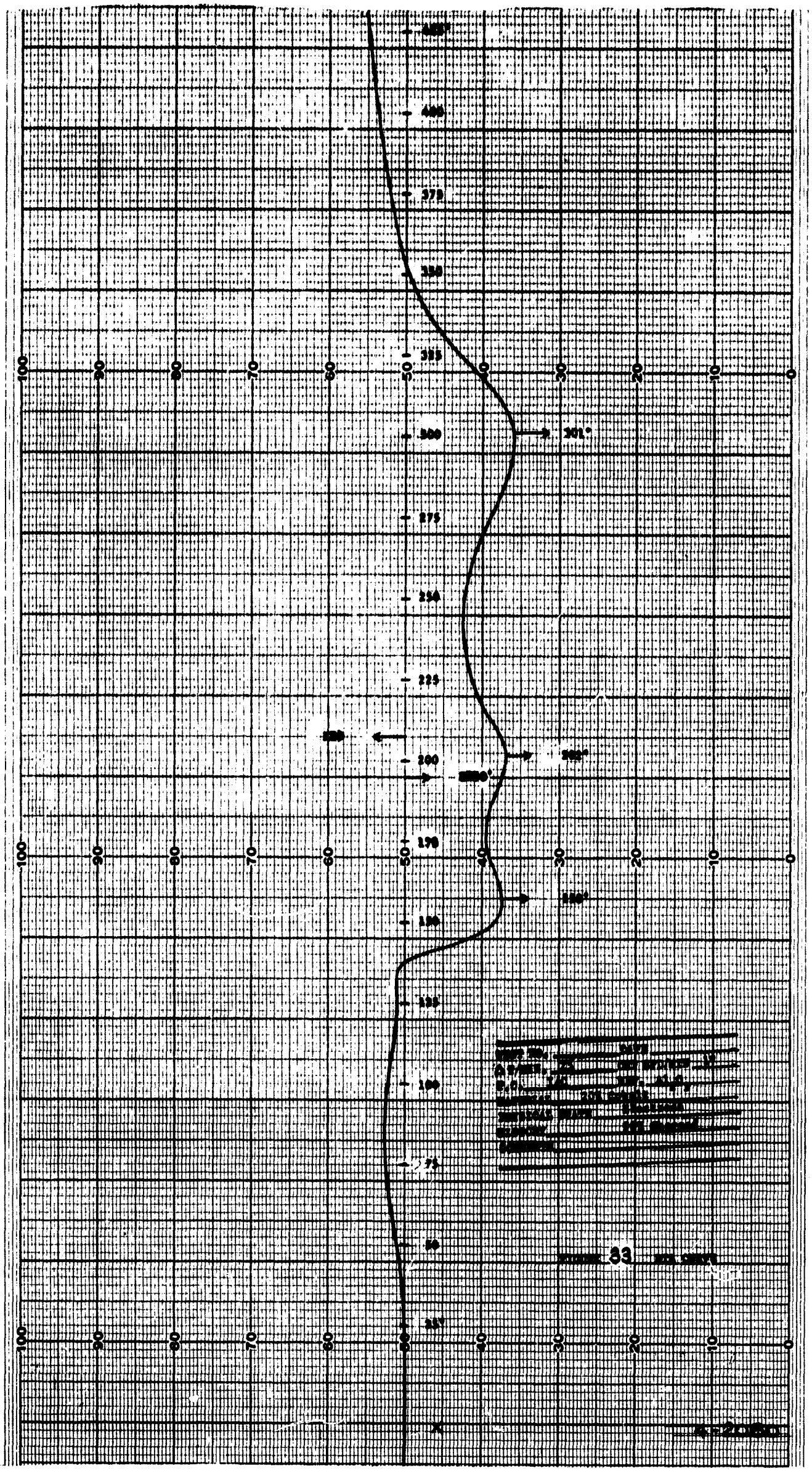
100
90
80
70
60
50
40
30
20
10
0
375
350
325
300
275
250
225
200
175
150
125
100
75
50
25
301°
202°
180°
183°
33

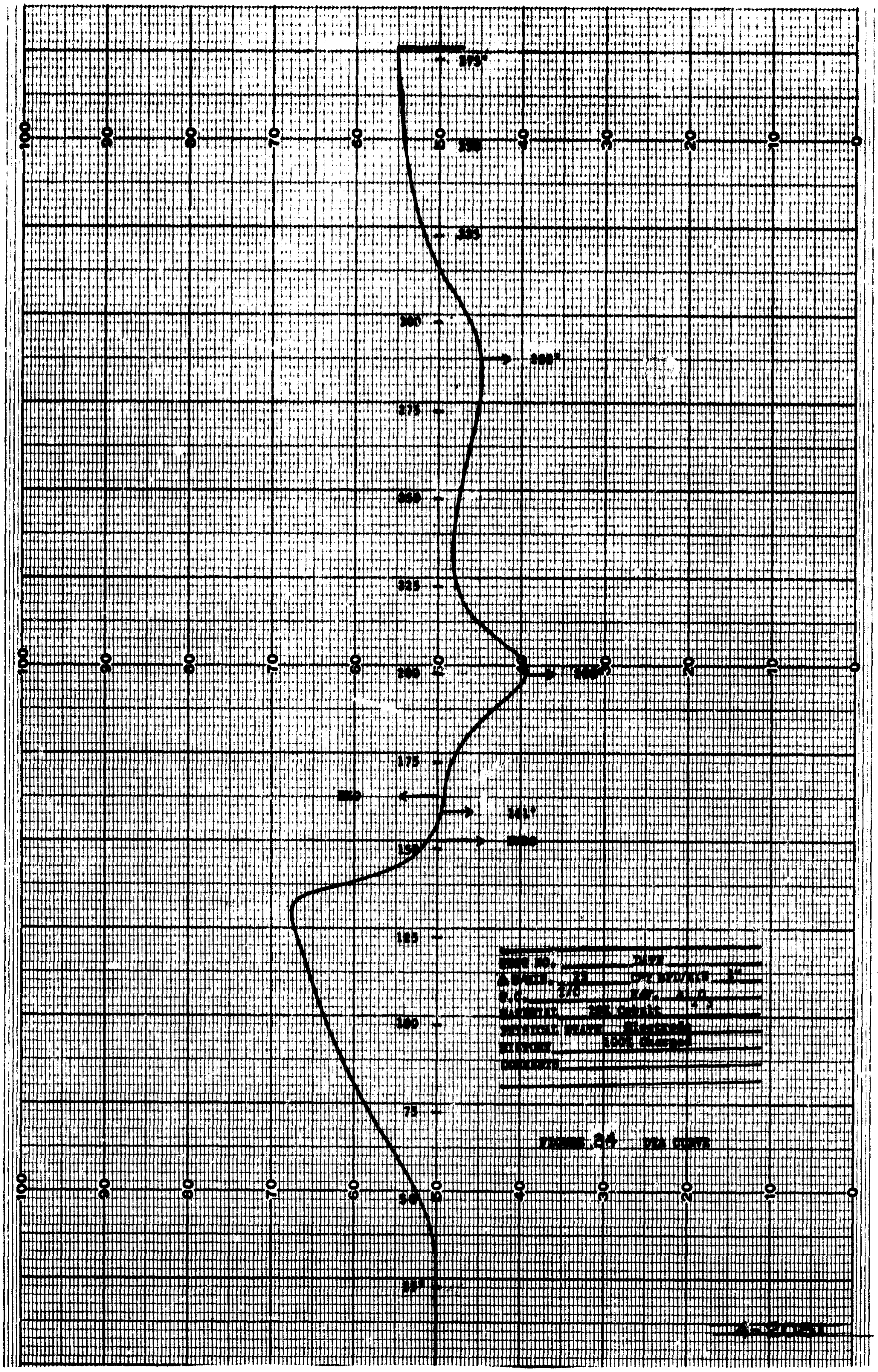

FIGURE 24 DTA CURVE

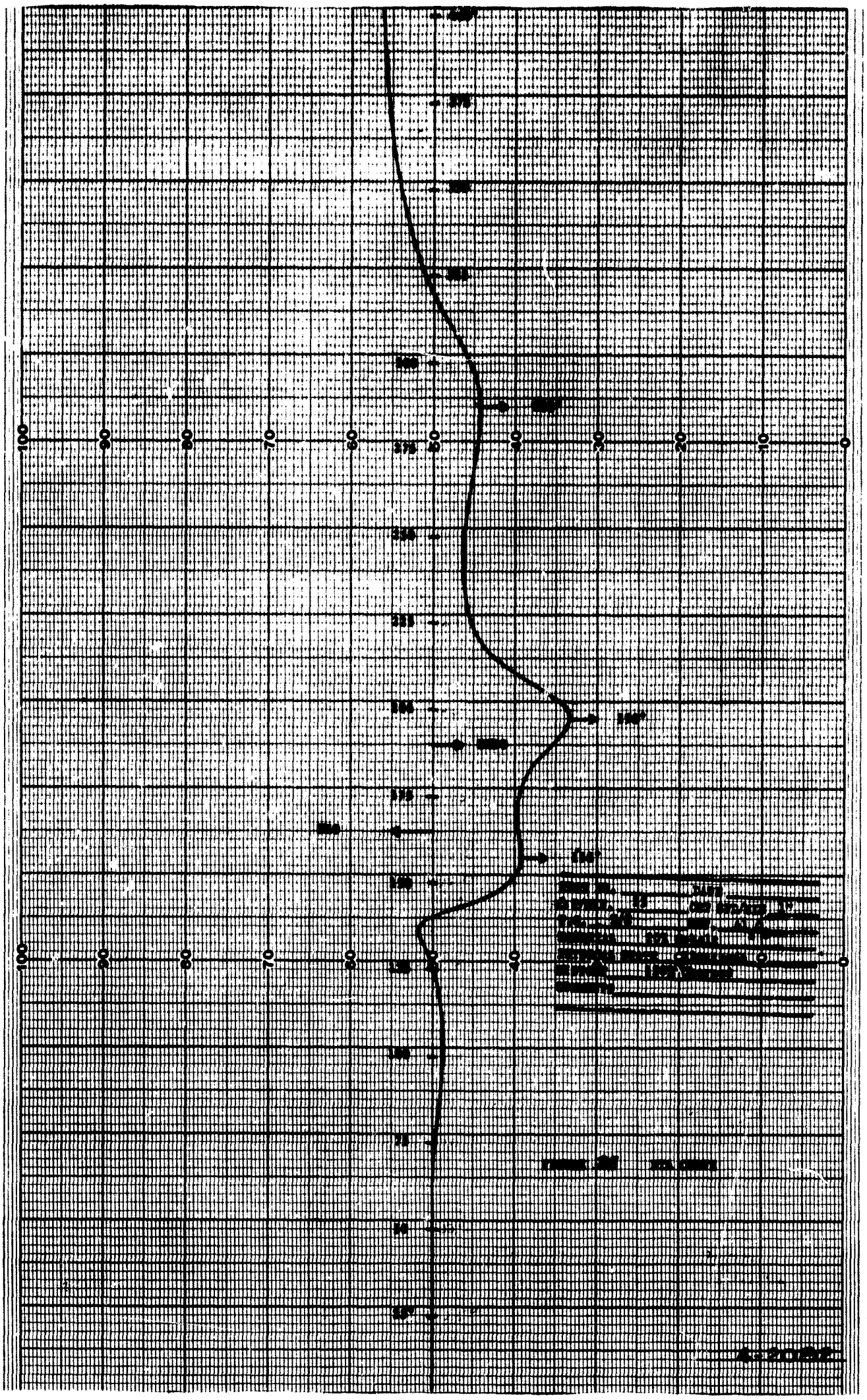

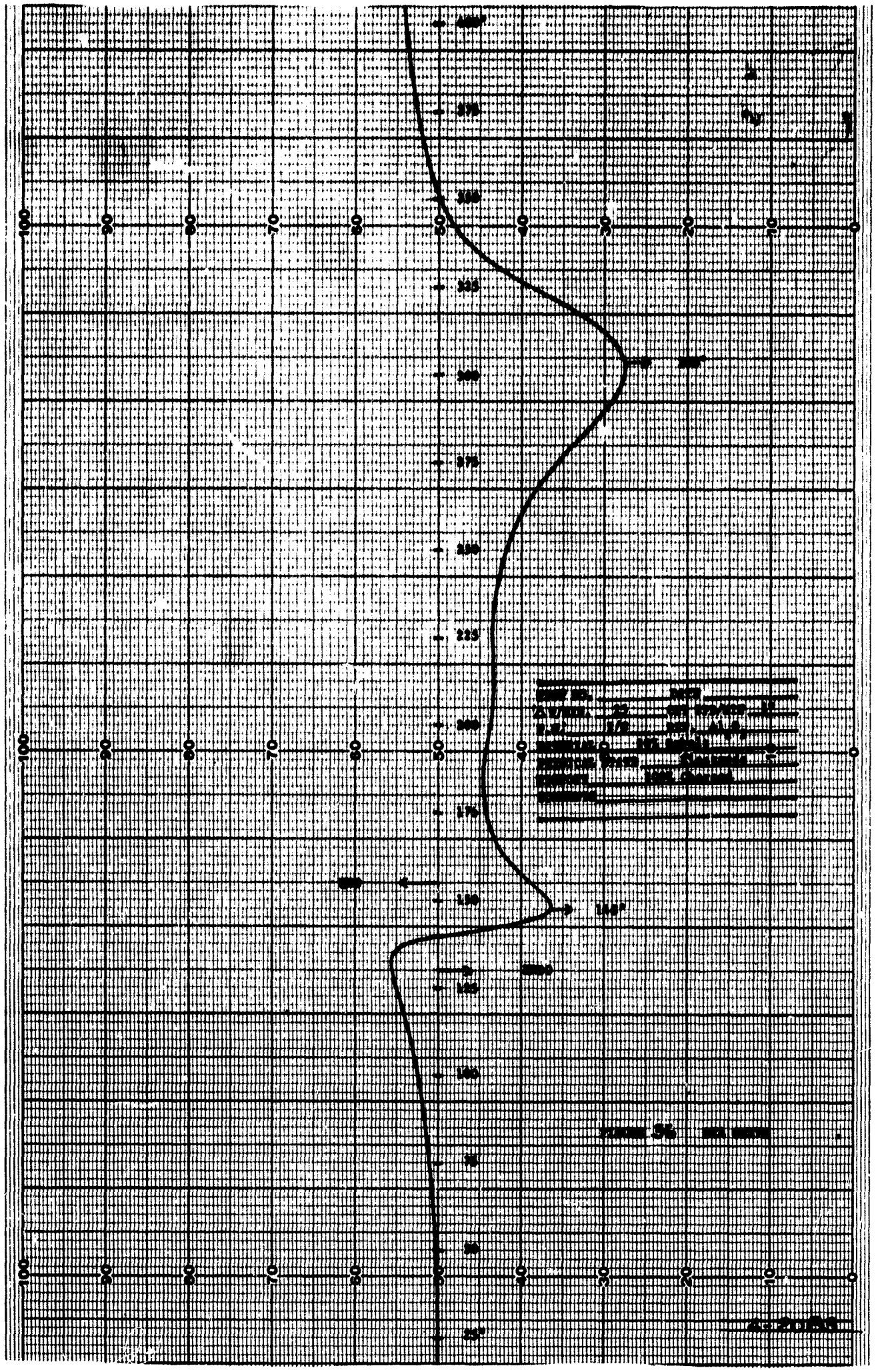

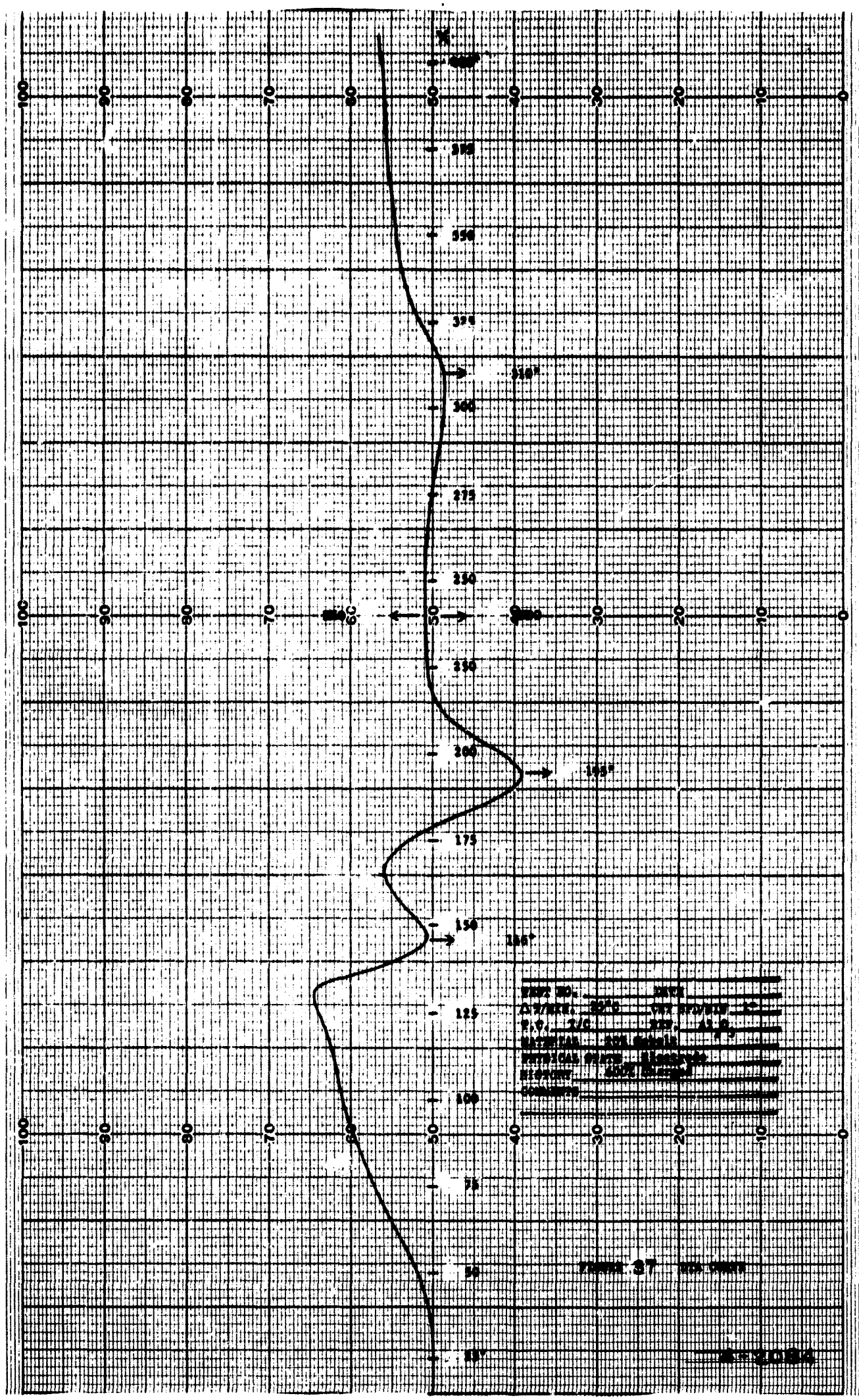
100
90
80
70
60
50
40
30
20
10
0
350
300
275
250
200
175
150
125
100
75
50
25
195°
156°
310°

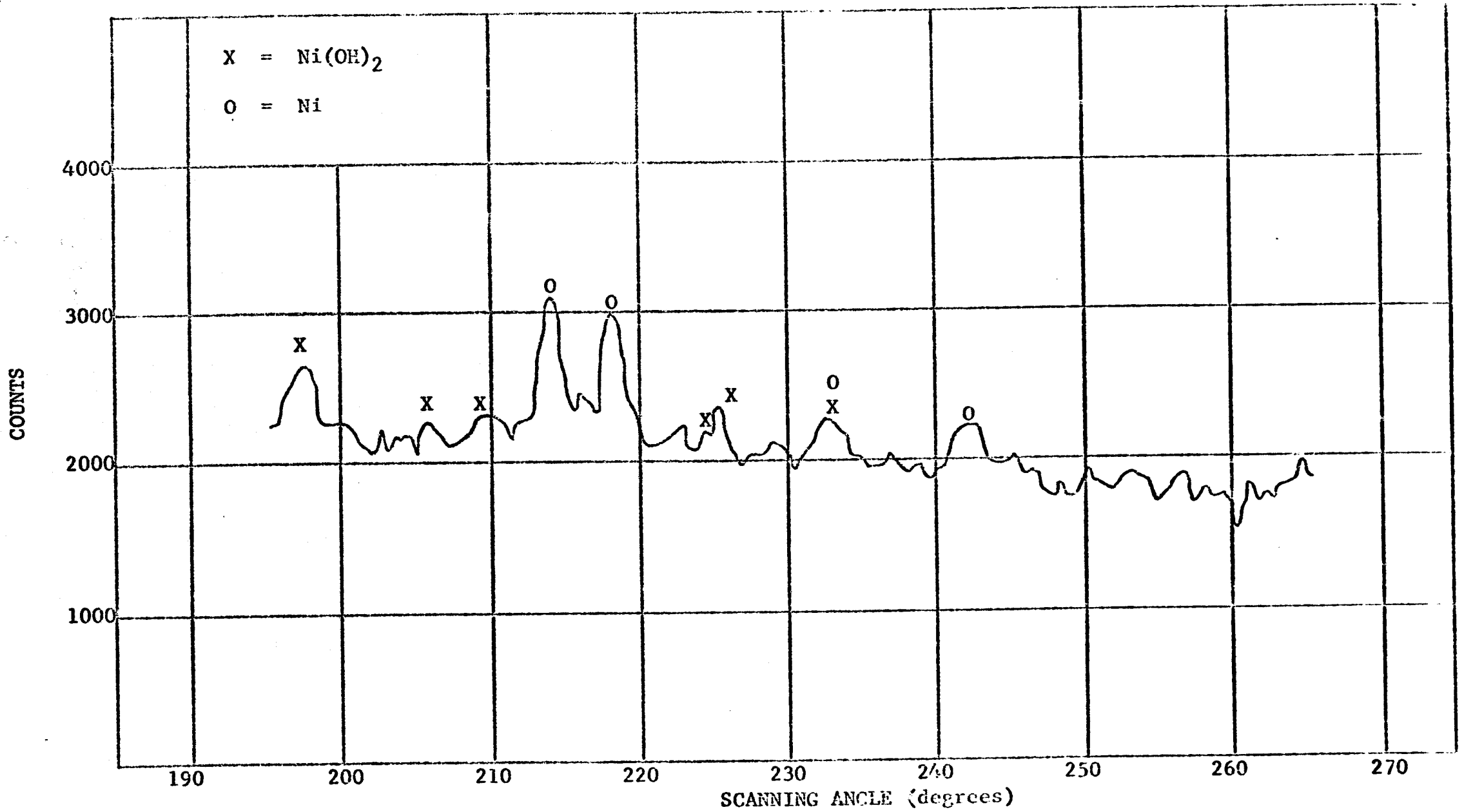

FIGURE 38 NEUTRON SPECTROMETER SCAN, POSITIVE ELECTRODE

4-2017